


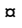
RESEARCH ARTICLE

Rab11A regulates dense granule transport and secretion during *Toxoplasma gondii* invasion of host cells and parasite replication

Kannan Venugopal¹[✉], Syla Chehade¹[✉], Elisabeth Werkmeister¹, Nicolas Barois¹[✉], Javier Periz², Frank Lafont¹, Isabelle Tardieux³, Jamal Khalife¹, Gordon Langsley⁴, Markus Meissner², Sabrina Marion¹^{*}

1 Univ. Lille, CNRS, Inserm, CHU Lille, Institut Pasteur de Lille, U1019—UMR 9017—CIIL—Center for Infection and Immunity of Lille, Lille, France, **2** Department of Veterinary Sciences, Experimental Parasitology, Ludwig-Maximilians-Universität, Munich, Germany, **3** Institute for Advanced Biosciences (IAB), Membrane Dynamics of Parasite-Host Cell Interactions, CNRS UMR5309, INSERM U1209, Université Grenoble Alpes, Grenoble, France, **4** Laboratoire de Biologie Comparative des Apicomplexes, Faculté de Médecine, Université Paris Descartes—Sorbonne Paris Cité, France, INSERM U1016, CNRS UMR8104, Institut Cochin, Paris, France

 These authors contributed equally to this work.

 Current address: Wellcome Centre for Integrative Parasitology, Institute of Infection, Immunity and Inflammation, University of Glasgow, Glasgow, United Kingdom

* sabrina.marion@pasteur-lille.fr



OPEN ACCESS

Citation: Venugopal K, Chehade S, Werkmeister E, Barois N, Periz J, Lafont F, et al. (2020) Rab11A regulates dense granule transport and secretion during *Toxoplasma gondii* invasion of host cells and parasite replication. PLoS Pathog 16(5): e1008106. <https://doi.org/10.1371/journal.ppat.1008106>

Editor: Michael J. Blackman, Francis Crick Institute, UNITED KINGDOM

Received: September 17, 2019

Accepted: February 10, 2020

Published: May 28, 2020

Copyright: © 2020 Venugopal et al. This is an open access article distributed under the terms of the [Creative Commons Attribution License](https://creativecommons.org/licenses/by/4.0/), which permits unrestricted use, distribution, and reproduction in any medium, provided the original author and source are credited.

Data Availability Statement: All relevant data are within the manuscript and its Supporting Information files.

Funding: KV, SM and GL have been supported by the Laboratoire d'Excellence (LabEx) ParaFrap from the National Agency for Research ANR-11-LABX-0024 grant and by the ANR-14-CE14-0002-01 grant. SM has been supported by a joint Chaire d'Excellence from Université of Lille and the Centre National pour la Recherche Scientifique (CNRS).

Abstract

Toxoplasma gondii possesses an armada of secreted virulent factors that enable parasite invasion and survival into host cells. These factors are contained in specific secretory organelles, the rhoptries, micronemes and dense granules that release their content upon host cell recognition. Dense granules are secreted in a constitutive manner during parasite replication and play a crucial role in modulating host metabolic and immune responses. While the molecular mechanisms triggering rhoptry and microneme release upon host cell adhesion have been well studied, constitutive secretion remains a poorly explored aspect of *T. gondii* vesicular trafficking. Here, we investigated the role of the small GTPase Rab11A, a known regulator of exocytosis in eukaryotic cells. Our data revealed an essential role of Rab11A in promoting the cytoskeleton driven transport of dense granules and the release of their content into the vacuolar space. Rab11A also regulates transmembrane protein trafficking and localization during parasite replication, indicating a broader role of Rab11A in cargo exocytosis at the plasma membrane. Moreover, we found that Rab11A also regulates extracellular parasite motility and adhesion to host cells. In line with these findings, MIC2 secretion was altered in Rab11A-defective parasites, which also exhibited severe morphological defects. Strikingly, by live imaging we observed a polarized accumulation of Rab11A-positive vesicles and dense granules at the apical pole of extracellular motile and invading parasites suggesting that apically polarized Rab11A-dependent delivery of cargo regulates early secretory events during parasite entry into host cells.

The funders had no role in study design, data collection and analysis, decision to publish, or preparation of the manuscript.

Competing interests: The authors have declared that no competing interests exist.

Author summary

Toxoplasma gondii (*T. gondii*) is a highly prevalent parasite infecting a wide range of animals as well as humans. *T. gondii* secretes numerous virulent factors contained in specific organelles, termed the rhoptries, micronemes and dense granules. These factors are released upon host cell recognition and enable parasite invasion and subsequent development into an intracellular vacuole. In particular, dense granules contain critical effectors that modulate intrinsic defenses of infected host cells ensuring parasite survival and dissemination. The mechanisms regulating dense granule secretion have not been elucidated. In this study, we unraveled a novel role for the *T. gondii* GTPase Rab11A in promoting dense granule transport along the parasite cytoskeleton and their content release into the vacuolar space during parasite replication. We also found that *T. gondii* Rab11A regulates extracellular parasite motility and adhesion to host cells suggesting a broader role in distinct secretory pathways essential for parasite virulence.

Introduction

Toxoplasma gondii (*T. gondii*) is an obligatory intracellular parasite that belongs to the phylum *Apicomplexa*, typified by the presence of specific apical secretory organelles called rhoptries and micronemes. Upon contact with the host cell, rhoptry (ROP) and microneme (MIC) proteins are released in order to promote parasite entry by driving the formation of a tight parasite-host cell adhesive membrane structure (termed the moving junction) [1]. ROP proteins also contribute to building the parasitophorous vacuole (PV), within which the parasite rapidly replicates. The molecular mechanisms regulating MIC exocytosis have been well studied leading to the discovery of specific parasite signaling pathways triggering their secretion upon parasite adhesion to host cells [2] [3]. Dense granules (DG) are also parasite secretory organelles critical for its survival, which release effectors modulating host immune and metabolic responses [4]. Dense granule proteins (GRA) also promote the formation of an intravacuolar nanotubular network (IVN), which interconnects parasites during intracellular replication, thereby ensuring the synchronicity of the successive divisions [5] [6] [7]. The IVN also connects the parasite to the PV membrane (PVM), presumably enhancing parasite exchanges with its host, notably for nutrient retrieval and parasite effector release into the host cytosol [8]. In contrast to micronemes and rhoptries, DGs are randomly distributed in the parasite cytosol and the mechanisms regulating their exocytosis at the parasite plasma membrane (PM) have not been elucidated. A recent study reported that in contrast to microneme exocytosis dense granule release is negatively regulated by cytosolic Ca^{2+} [9]. In Metazoan, the process of exocytosis implies the [active transport](#) of secretory vesicles to the PM, and the secretion of their content into the extracellular environment or their insertion into the PM. In mammalian cells and plants, two different exocytic routes have been described: the “constitutive secretory pathway” supports the sorting of newly synthesized proteins from the endoplasmic reticulum, through the [Golgi apparatus](#) to the PM. By contrast, the “recycling pathway” targets to the cell surface internalized material that has been transported to and sorted in the perinuclear or peripheral recycling endosomes [10]. In *T. gondii*, DGs are considered to be the default constitutive secretory pathway based on the observation that the SAG1-GFP fusion protein (full product or truncated of its GPI anchor (SAG1ΔGPI)) is transported within DGs before being released into the vacuolar space [11]. In addition, proteins whose specific motifs targeting them to other secretory organelles have been deleted are localized in DGs [12] [13]. Yet, there is so far

no evidence that transmembrane proteins navigate through the DGs to reach the parasite's PM.

The Rab GTPases belong to the Ras small G protein subfamily and operate as molecular switches that alternate between two conformational states: the GTP-bound "active" form and the GDP-bound "inactive" form [14]. Through their interactions with various effectors, such as coat components, molecular motors, and soluble NSF attachment protein receptors (SNAREs), Rab GTPases serve as multifaceted organizers of almost all membrane trafficking processes, including vesicle budding from the donor compartment, vesicle transport along cytoskeleton tracks and vesicle tethering and fusion at the acceptor membrane [14] [15] [16]. Among the Rab GTPases, Rab11 regulates both constitutive secretory and recycling pathways, thus controlling secretion at the PM [15] [16] [17]. In mammalian cells, Rab11 promotes vesicle transport via their anchoring to both, microtubule [18] and actin-based [molecular motors](#) [19]. In addition, Rab11A promotes the tethering of recycling vesicles to the PM in concert with the exocyst complex [20] [21] [22]. Through multiple interactions with effector molecules, Rab11 influences numerous cellular functions including ciliogenesis [23], cytokinesis [24], and cell migration [25] [26]. In contrast to humans, which express over 70 Rabs, *T. gondii* possesses a limited number of 13 Rabs that include two isoforms of Rab11: Rab11A and Rab11B [27]. In *T. gondii* as well as in the related apicomplexan genus *Plasmodium*, Rab11A-defective parasites are unable to complete cytokinesis and show marked defects in the exocytosis-assisted process that leads to proper individualization of daughter cells, otherwise posteriorly connected [28] [29] [30]. In *Plasmodium*, this process was suggested to be regulated by PI4K-Rab11A-mediated secretion of vesicles from the Trans-Golgi Network (TGN) to the PM [29] [30]. Here, we further explored the functions of Rab11A in *T. gondii* and demonstrated its key role in regulating DG exocytosis and transmembrane protein delivery at the parasite PM. We also unraveled a novel role for Rab11A in extracellular parasite adhesion and motility, thereby contributing to host cell invasion.

Results

Rab11A localizes to dynamic cytoplasmic vesicles

To investigate *T. gondii* Rab11A localization, we raised a polyclonal antibody in mice, which recognized a unique protein of the expected size of 25kDa in a total extract of type I RHΔ*Ku80* parasites (Fig 1A). Next, we performed immunofluorescence assays (IFA) in fixed RHΔ*Ku80* tachyzoites. Rab11A displayed distinct localizations depending on the cell cycle stage. During the G1 phase, Rab11A was localized in cytoplasmic vesicles and as previously described [28], a signal was also detected at the Golgi/Endosome-Like Compartment (ELC) region (Fig 1B). IFA confirmed the co-distribution of Rab11A with the TGN marker *TgSortilin-like Receptor* (*TgSORTLR*) (S1 Fig). Consistent with this observation, Rab11A was found to be mostly localized adjacent to the Rab5A signal defining the early ELC, previously shown to be tightly associated with the TGN [31] (S1 Fig). During cytokinesis, the Golgi localization of Rab11A was also detected in emerging daughter cells, together with a strong enrichment of the protein at the apical tip of the growing buds, reflecting a possible Rab11A-dependent transport of newly synthesized material between these two locations (Fig 1B and S1B Fig). Rab11A also accumulated at the basal pole of the parasite at the end of cytokinesis (Fig 1B).

In order to get further insights into the dynamic localization of Rab11A, we used the previously established transgenic ddFKBP-myc-mCherryRab11A-RHΔ*Ku80* parasites (from here designated as mcherryRab11A-WT parasites) [28] [32]. In this strain, the expression of Rab11A fused to a mCherry tag is under the control of an N-terminal ddFKBP tag, which allows regulation of recombinant protein levels by the inducer Shield-1. Using super-

Fig 1. A- Western blot analysis with specific anti-Rab11A antibodies detects a unique band at 25kDa in a RHΔKU80 parasite lysate. B- Analysis of Rab11A localization in fixed RHΔKU80 parasites using antibodies recognizing Rab11A, IMC3 and ROP2/3, as indicated. Bars: 1 μm. C- Sequences of images extracted from *S1 Movie* and *S2 Movie* (left images, white frames) showing the dynamic bi-directional movement of Rab11A-positive vesicles in the cytosol (upper sequence) and along the parasite cortex (lower sequence) of mcherryRab11A-WT and IMC3-YFP expressing parasites. Tracking of vesicle trajectory is also shown. Images on the right show a zoom of the residual body (RB) region indicated by a yellow frame in the corresponding vacuoles. The arrow indicates Rab11A-positive tubular-like structures connecting the parasites Bars: 2 μm. D- Sequences of images extracted from *S5 Movie* and *S6 Movie* (left images, white frames) showing the dynamic movement of Rab11A-positive vesicles along the parasite cortex (upper sequence) and in the cytosol (lower sequence) of mcherryRab11A-WT and Cb-Emerald GFP (Cb-E) expressing parasites. Bars: 2 μm. E- Images extracted from movie *S7 Movie*. mcherryRab11A-WT and IMC3-YFP expressing parasites were treated with cytochalasin D (CD) for 30 min before being recorded. Rab11A-positive vesicles are detected in clusters displaying confined trajectories (right image: “tracking”). Bar: 2 μm.

<https://doi.org/10.1371/journal.ppat.1008106.g001>

resolution live imaging of parasites expressing the Inner Membrane Complex protein IMC3-YFP and mCherryRab11A-WT, we clearly observed bi-directional trajectories of Rab11A-positive vesicles between the basal and apical poles of the parasite both within the parasite cytosol (*Fig 1C* and *S1 Movie*) and along the parasite cortex delineated by the IMC3-YFP staining (*Fig 1C* and *S2 Movie*). During cytokinesis, videomicroscopy highlights the presence of Rab11A at the Golgi area of daughter cells and the transport of Rab11A-positive vesicles along the newly formed daughter bud scaffold (*S3 Movie*). In addition, consistent with our IFA imaging, we detected a dynamic localization of Rab11A at the basal pole of replicating parasites (*S4 Movie*). Interestingly, we also noticed Rab11A-positive vesicles and tubular-like structures within the residual body region (*Fig 1C*, RB). This region has been recently described to harbor a dense actino-myosin network that interconnects intracellular dividing tachyzoites [6] [7], suggesting that Rab11A may regulate actin-dependent material exchanges between parasites, or the dynamics of this cell-to-cell connecting network. In line with this observation, after transient expression of actin chromobodies coupled to Emerald GFP (Cb-E) that specifically label filamentous actin [7], we visualized Rab11A-positive vesicles moving along actin-positive structures at the parasite cortex (*Fig 1D*, upper panel and *S5 Movie*) or anchored to dynamic F-actin structures within the parasite cytosol (*Fig 1D*, lower panel and *S6 Movie*). As previously observed [7], we also detected dynamic F-actin structures at the Golgi/ELC area that co-distribute with the Rab11A signal (*S5 Movie*). To investigate whether Rab11A-positive vesicle movements depend on the actin cytoskeleton, we treated IMC3-YFP/mcherryRab11A-WT tachyzoites with cytochalasin D (CD) for 30 min before recording parasites by live imaging. Depolymerizing actin filaments by CD led to the formation of cytosolic and cortical Rab11A-positive clusters that in contrast to non-treated parasites, displayed confined trajectories as illustrated by the tracking of their displacement (*Fig 1E* “tracking”, *S7 Movie*).

Collectively, these data demonstrated that Rab11A-positive vesicle movement is dependent on actin cytoskeleton activity and that Rab11A might participate in (i) vesicle budding from the TGN/ELC, (ii) cargo transport between the apical and basal poles of the parasite and (iii) material exchange between the replicating parasites via release of vesicles at the basal pole.

Rab11A-positive vesicles dynamically co-distribute with DGs

The DG-mediated secretory pathway is considered in *T. gondii* to be the default constitutive secretory pathway based on the observation that soluble SAG1 protein truncated of its GPI anchor (SAG1ΔGPI) is transported within DGs before being released into the vacuolar space [10] [33]. Interestingly, the dynamic motion of Rab11A-positive vesicles was similar to recently described actin and myosin F-dependent movements of DGs [33] and Rab11A is known as a regulator of exocytosis in other eukaryotic systems [15].

In order to explore dense granule dynamics in relation to Rab11A, we expressed SAG1ΔGPI-GFP in mcherryRab11A-WT parasites. Using live imaging, we confirmed that DG content

was efficiently released, as illustrated by the localization of the GFP signal in the vacuolar space (Fig 2A). GFP-positive DGs detected in the parasite cytosol displayed a significant and dynamic co-distribution with mCherryRab11A-WT positive vesicles (Fig 2B and 2C). In replicating parasites, 33,7% of the DG population co-distributed over time with Rab11A-positive vesicles, while 26,1% of Rab11A-positive vesicles co-distributed with DGs. This shows that Rab11A-positive vesicles and DGs are distinct intracellular compartments that transiently interact with each other. Consistent with this notion, fluorescent signal intensity profiles indicated that GFP-positive DGs and mCherryRab11A-positive vesicles are closely apposed (Fig 2A and 2B). This is also clearly visualized in S8 Movie (Fig 2D), in which a DG is observed docked onto a Rab11A-positive vesicle, the latter being anchored at the periphery of the parasite, and both compartments are simultaneously transported along the parasite cortex (Fig 2D). We tracked this GFP-positive DG motion (Fig 2E and 2F; S9 Movie and S10 Movie) and fitted the recorded xy positions over time using mathematical models of “directed” or “diffusive” motion (see M&M) [34]. We confirmed that the DG trajectory 2 is consistent with “directed” motion (fitted curve, Fig 2F) characteristic of a vesicle moving along cytoskeleton tracks, in contrast to the trajectories 1 and 3, characteristic of “confined” diffusive motions [34]. This together with the observed inhibition of Rab11A-positive vesicle and DG movements upon CD treatment (Fig 1D) [33], suggests that Rab11A promotes DG transport by mediating their anchoring along actin filaments, at least at the parasite cortex.

Rab11A promotes DG exocytosis

To assess whether Rab11A regulates DG transport, docking or the later step of fusion at the PM, we used a previously established parasite strain that over-expresses in a rapidly inducible manner an inactive GDP locked version of Rab11A fused to the mCherry fluorescent reporter (DDmCherrycmycRab11A-DN-RHΔKu80; from hereon called mCherryRab11A-DN and distinguished from mCherryRab11A-WT) [28] [32]. By WB, we confirmed that both Rab11A-WT and Rab11A-DN proteins were expressed in similar amounts after 4 h induction with Shield-1 (Fig 3A). First, we monitored DG release in fixed Rab11A-WT and Rab11A-DN intracellular tachyzoites following gentle saponin permeabilization, which improved detection of secreted GRA proteins localized in the vacuolar space and at the PVM. To rule out any indirect effect of the previously described cytokinesis defect on DG secretion in Rab11A-DN parasites [28], we pre-treated freshly egressed extracellular tachyzoites for 1 h with Shield-1 before seeding them on a fibroblast monolayer and analyzed DG secretion 2h and 4h after parasite invasion (Fig 3B). We observed a drastic block of GRA1 and GRA3 secretion in Rab11A-DN parasites in contrast to Rab11A-WT in which both proteins were typically released in the vacuolar space or decorated the PVM (Fig 3B and 3C). A similar observation holds for additional GRA proteins (GRA2, GRA5 and GRA16) as shown in S2 Fig. Notably, in contrast to Rab11A-WT parasites, GRA16-positive DGs were also retained within Rab11A-DN parasite cytosol and accordingly GRA16 no longer reached the host cell nuclei 16h post-infection [35] (S2B Fig).

To further analyze the role of Rab11A in DG secretion, we also expressed SAG1ΔGPI-GFP in mCherryRab11A-DN parasites. In contrast to Rab11A-WT parasites, Rab11A-DN parasites were impaired in their ability to release SAG1ΔGPI-GFP into the PV space (Fig 3D). Consequently, DGs were densely packed in the cytosol, which impaired reliable automatic tracking of all vesicles and therefore the quantification of the percentage of “directed” versus “diffusive” or “confined” trajectories in the total DG population. Nonetheless, DGs appeared to mostly display diffusive and confined motions (Fig 3E: tracking of 4 DG and their resulting trajectories shown in S11 Movie, which were further analyzed in Fig 3F). In particular, the

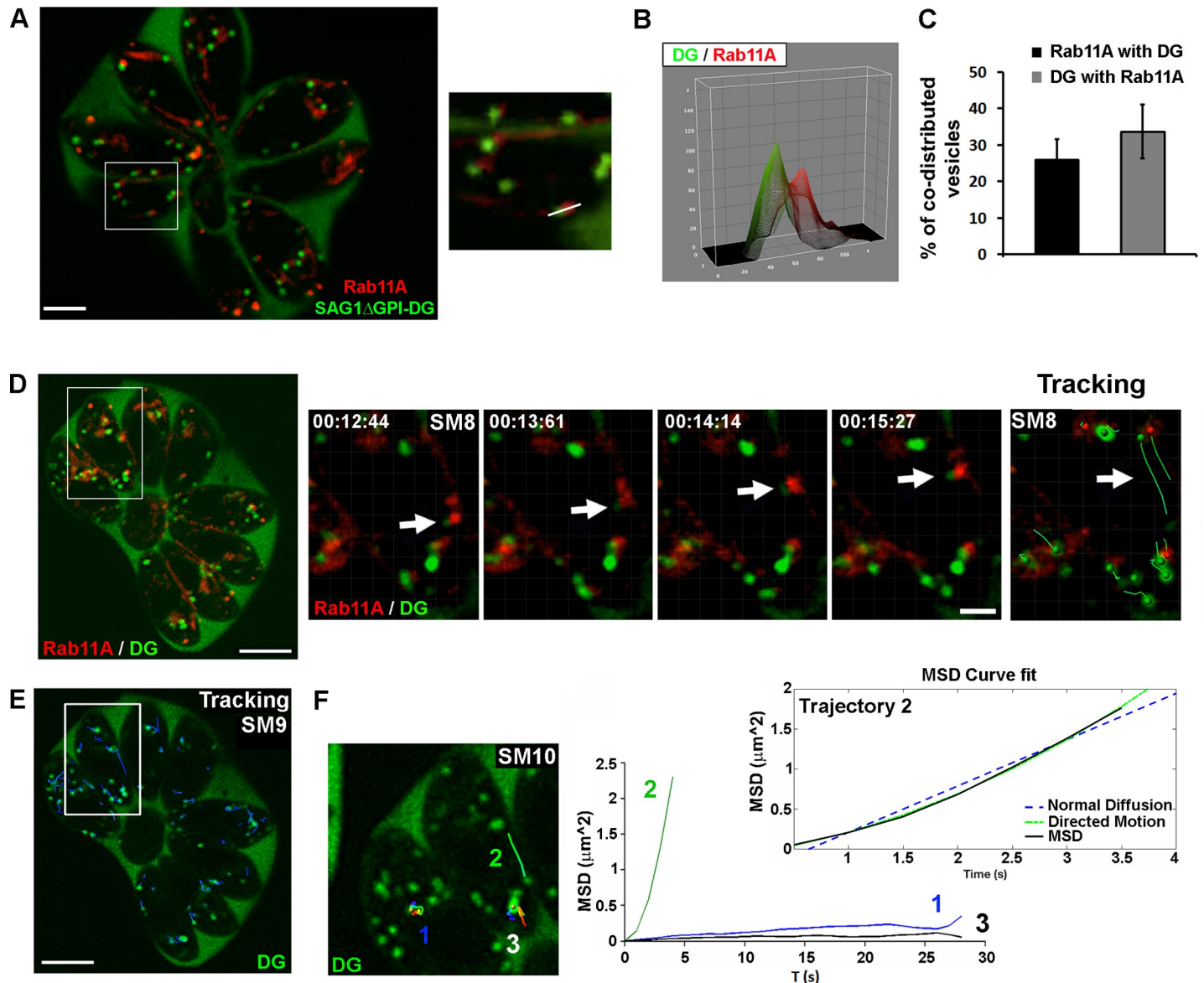


Fig 2. A- Image extracted from a time-lapse acquisition illustrating the release of SAGΔGPI protein (green) into the vacuolar space of mcherryRab11A-WT and SAGΔGPI-GFP expressing parasites, as well as the co-distribution in the parasite cytosol of SAGΔGPI-GFP positive DG (green) and mcherryRab11A-WT positive vesicles (red). The right insert shows a zoom of the region indicated by a white frame in the full vacuole. Bar: 2 μm. B- Fluorescence intensity profiles plotted over the distance of the GFP and mcherry signals along the line indicated in A (insert). C- Percentage of co-distribution between the total population of SAGΔGPI-GFP-positive DGs and mcherryRab11A-WT-positive vesicles of a given vacuole averaged over 5 consecutive time points (n = 10 vacuoles). Data show mean ± SD. D- Sequences of images extracted from S8 Movie (region indicated by a white frame in the full vacuole) showing the joint motion of a Rab11A-positive vesicle (red) and a SAGΔGPI-positive DG (green) along the parasite cortex, as illustrated by their tracking (S8B Movie). Time is indicated in seconds. E- Automated tracking of all DG trajectories within the vacuole (S9 Movie). F- Three trajectories (1, 2, 3) (S10 Movie) in the region indicated by a white frame in E- were analyzed by plotting the Mean Square Displacement (MSD) over ΔT (s) using the Imaris software. Trajectory N² (black line) corresponding to the track shown in -D (S8 Movie) fitted a mathematical model of “directed” motion (green line) defined by the equation $MSD = 4Dt + v^2t^2$ while trajectories 1 and 3 display confined motions.

<https://doi.org/10.1371/journal.ppat.1008106.g002>

accumulation of DGs observed at the altered interface between the two segregating daughter cells accounted for a local *quasi* static behavior as illustrated by their confined trajectories (Fig 3F: trajectories 2, 3 and SM11). Rare longer trajectories could be detected along the cortex of the parasites (such as illustrated for trajectory 1), however they never fitted, with good probability, a model of directed motion. In agreement, analysis of cortical DG trajectories in

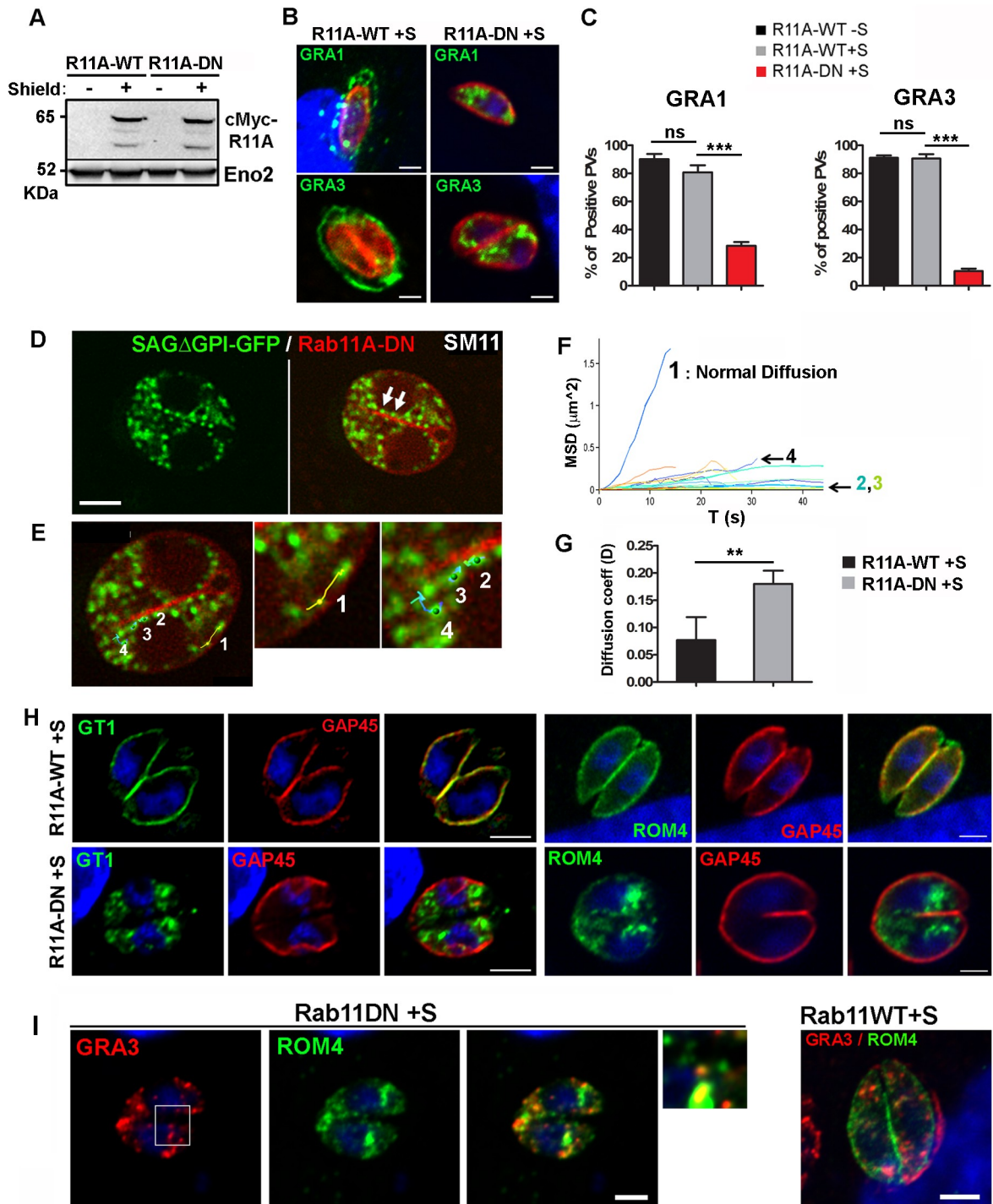


Fig 3. A- Western blot analysis using anti-Rab11A antibodies showing Rab11A-WT and Rab11A-DN proteins in similar amounts after 4 h of Shield-1 induction (+S) of intracellular tachyzoites. Eno2 is used as a loading control. B- Immunofluorescence assay (IFA) showing the dense granule proteins GRA1 and GRA3 (green) retained in intra-cytosolic vesicles following 2 h (upper panel) and 4 h (lower panel) of Shield-1 induction of Rab11A-DN parasites, while being efficiently released into the vacuolar space and at the vacuole membrane in similarly induced Rab11A-WT parasites. The parasite cortex is delineated by the glideosome protein GAP45 (red). Bars: 1 μm. C-Percentage of vacuoles positive for GRA1 and GRA3 secretion in Rab11A-WT and Rab11A-DN parasites induced (+S) or not (-S) with Shield-1. Data show mean ± SEM of three independent experiments (unpaired Student's *t*-test, GRA1: ****p* < 0.0001 et GRA3: ****p* = 0.0008). D- Image extracted from [S11 Movie](#) illustrating DG movements in mcherryRab11A-DN (red) / SAGΔGPI-GFP expressing parasites. DGs accumulate in the parasite cytosol or remain stationary along the segregating membrane of daughter cells (arrows). Bar: 2 μm. E- Images extracted from [S11 Movie](#) showing the tracking of 4

DGs and their resulting trajectories, which were analyzed in F-. F- Tracking of DGs in Rab11A-DN expressing parasites indicates mostly confined (as exemplified for DG trajectories 2, 3) and diffusive (trajectories 1, 4) motions. G- Mean diffusion coefficient (D) calculated from 10 cortical trajectories manually tracked in Shield-1 induced Rab11A-WT and Rab11A-DN parasites. Data show mean \pm SD (unpaired Student's *t*-test ** $p < 0.01$). H- IFA showing the glucose transporter GT1 and Romboid protein ROM4 (green) retained in intra-cytosolic vesicles in Shield-1 induced Rab11A-DN parasites, while being efficiently delivered at the plasma membrane in induced Rab11A-WT parasites. The parasite cortex is delineated by GAP45 (red). Bars: 2 μ m. I- IFA showing the localization of the proteins GRA3 (red) and ROM4 (green) in distinct vesicles in Shield-1 (+ S) induced Rab11A-DN expressing parasites during parasite replication. In Rab11A-WT expressing parasites, GRA3 and ROM4 localized at the vacuolar membrane and at the parasite plasma membrane, respectively. Bars: 2 μ m.

<https://doi.org/10.1371/journal.ppat.1008106.g003>

Rab11A-WT and Rab11A-DN parasites revealed a significant increase in the coefficient of diffusion of Rab11A-DN trajectories, suggesting a role for Rab11A in regulating DG directed transport along the parasite cytoskeleton (Fig 3G). Finally, we performed an experiment in which we washed out 0.5 μ M- (S12 Movie) or 1 μ M- (S13 Movie) Shield-1 pre-induced Rab11A-DN parasites in order to arrest the expression of the Rab11A-DN protein. We clearly observed, 4h after Shield-1 removal, a strong accumulation of GFP-positive DGs at the parasite PM together with the re-initialization of their content release (S12 Movie), and a pronounced signal at the defective interface between dividing parasites (S13 Movie). This observation suggests that Rab11A may be required for DG docking/tethering at the PM.

Collectively, these data indicate that Rab11A regulates both the directed transport of DG along cytoskeleton tracks (Fig 1D and Fig 2D, 2E and 2F) and their exocytosis into the PV space.

Rab11A regulates transmembrane protein localization at the PM

Based on our previous study [28], we proposed that Rab11A is required for the delivery of vesicles containing SAG1 and probably other surface proteins, from the endosomal network to the plasmalemma of daughter cells, where new PM is synthesized, similar to its function described in other eukaryotes. This prompted us to investigate whether during replication Rab11A might regulate the localization of other surface proteins in *T. gondii*. We transiently transfected Rab11A-WT and -DN parasites with plasmids encoding the transmembrane HA-tagged Glucose transporter 1 (GT1) [36], or the Ty-tagged rhomboid protease 4 (ROM4) [37]. In contrast to the rhomboid protease ROM1 that localizes to micronemes, ROM4 was found to be targeted to the tachyzoite PM, suggesting that it is transported through the constitutive pathway [37] [38]. Similar to DGs, GT1 and ROM4 proteins were retained in intracellular vesicles and were no longer delivered to the parasite PM (Fig 3H). In addition, we took advantage of the impaired exocytosis activity in Rab11A-DN parasites to study whether different populations of secretory vesicles may co-exist during parasite replication. Co-localization studies in fixed Rab11A-DN parasites showed that ROM4 and GRA3 partially co-localize, but were also detected in distinct vesicular compartments (Fig 3I). This may reflect a distinct timing of protein synthesis and vesicle release from the Golgi to the PM. However, this observation also suggests the existence of different regulatory pathways for the trafficking of protein localized at the PM vs proteins secreted into the vacuolar space. In particular, transmembrane proteins may be actively recycled during parasite division, as suggested in a previous study on the retromer subunit TgVPS35 [39], and more recently during extracellular parasite motility [40]. Thus, Rab11A may not only play a role in the regulation of DG protein release into the vacuolar space but also in the trafficking of proteins localized at the PM during parasite replication.

Importantly, unlike GRA protein secretion, DG biogenesis was not impaired in Rab11A-DN parasites as assessed by transmission electron microscopy (Fig 4). In addition, supporting a major disturbance in DG exocytosis, the IVN could not be detected in the drastically reduced vacuolar space characterized by the PVM being closely apposed to the parasite

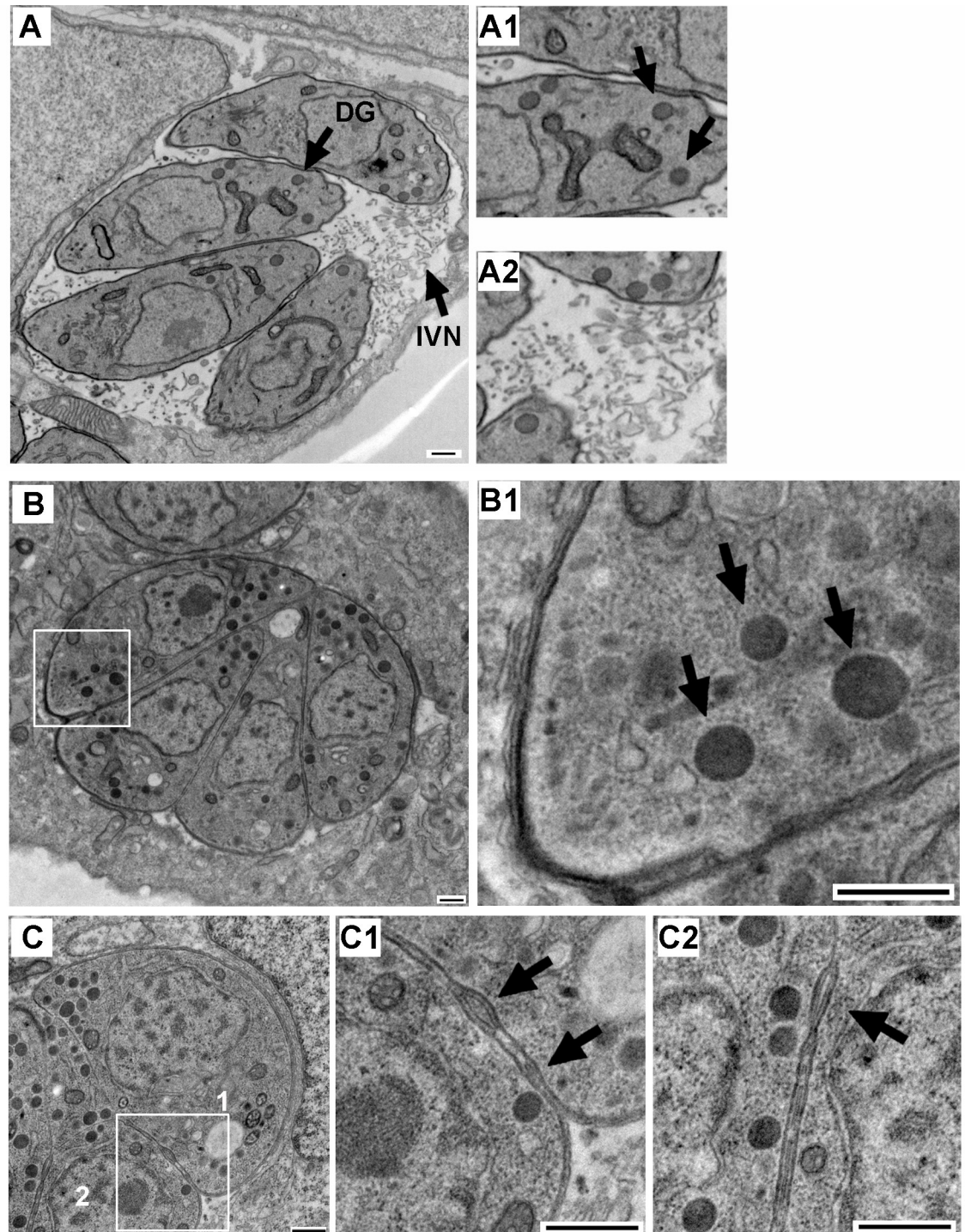


Fig 4. Electron micrographs of infected host cells harboring Shield-1 induced Rab11A-WT replicating parasites (A), in which dense granules (A1) and the IVN (A2) are visualized. Shield-1 induced Rab11A-DN parasites (B-C) accumulate dense granules (B and B1: a zoom of the region indicated by a white frame in B) and the IVN is not detected in the drastically reduced vacuolar space (B). Rab11A-DN expressing parasites also display a previously described defect in membrane segregation between daughter cells (C). A zoom of the regions 1 and 2 is shown in C1 and C2. Bars: 500nm.

<https://doi.org/10.1371/journal.ppat.1008106.g004>

PM (Fig 4B and 4C). We also detected the previously described defect in daughter cell segregation [28] (Fig 4C, arrows). Presumably, in addition to the contribution of the mother cell plasma membrane, delivery of new membrane is required to complete daughter cell segregation at the end of cytokinesis and this process may be regulated by Rab11A. In line, the requirement for *de novo* lipid synthesis to complete daughter cell segregation has been already demonstrated in other studies [41].

Rab11A regulates adhesion and motility of extracellular parasites

A role for Rab11A in parasite invasion has been previously demonstrated [32]. To explore which steps of parasite entry (e.g. adhesion, motility, and invasion) were altered, we treated extracellular Rab11A-WT and -DN parasites with Shield-1 for 2 h before monitoring their ability to adhere to host cells. We found that Rab11A-DN tachyzoites were severely impaired in surface attachment to human fibroblast (HFF) monolayers compared to Rab11A-WT parasites (Fig 5A). Furthermore, parasites that successfully adhered exhibited a strong defect in motility, as quantified by the percentage of parasites displaying a SAG1-positive trail deposit (Fig 5B). Importantly, compared to Rab11A-WT parasites, the morphology of adherent motile Rab11A-DN parasites was altered, the latter being wider and shorter, losing their typical arc shape (Fig 5C). Analysis of individual parasites imaged by Scanning EM ($n = 70$ for WT and DN) confirmed that Rab11A-DN parasites display a significant increase in circularity and accordingly, a decrease in the aspect ratio (AR: major axis/minor axis) (Fig 5D). Of note, conoid extrusion was only slightly decreased in Shield-1 induced Rab11A-DN compared to Rab11A-WT (Fig 5E). Along this line, changes in morphology were not correlated with major perturbations in formation and organization of the sub-pellicular microtubule network in Rab11A-DN parasites compared to Rab11A-WT (Fig 5F).

An impaired recruitment of late glideosome components at daughter cell buds has been previously reported in dividing Rab11A-DN parasites [28] and could account for the motility defect. However, we induced Rab11A-DN protein expression in non-dividing extracellular parasites and accordingly we did not observe any significant defect in the localization of GAP45 and Myosin Light Chain 1 (MLC1) at the cortex of extracellular parasites (S3 Fig). This indicates that the morphological defect observed in Rab11A-DN parasites is not correlated with a significant perturbation of glideosome component localization.

The microneme protein MIC2, a transmembrane protein released at the PM of the parasite, promotes parasite motility and adhesion [42] [43]. First, we confirmed by IFA that MIC2-positive micronemes were detected at the apical pole of extracellular induced Rab11A-DN parasites, indicating no defect in their formation and localization (S4A Fig). Secretion of microneme proteins by extracellular parasites can be triggered by ethanol, a step followed by their release from the parasite PM after cleavage by proteases. Notably, ROM4 has been shown to promote MIC2 trimming at the parasite PM [38]. Since ROM4 was no longer present at the PM of replicating Rab11A-DN parasites, we investigated whether a similar defect could be observed in 2h Shield-1 induced extracellular Rab11A-DN parasites. As previously observed for glideosome components, ROM4 localization at the PM was not perturbed in extracellular induced Rab11A-DN parasites (S4B Fig). Next, we performed excretion/secretion assays to assess the transport of the MIC2 protein to the parasite PM and its subsequent release into the culture medium. Western blot quantification of the Excreted-Secreted Antigen (ESA) fractions demonstrated a significant reduction in MIC2 release upon induction of microneme exocytosis by ethanol (Fig 5G). Accordingly, a slight increase in MIC2 protein levels was observed in the pellet fraction, also indicating that the decrease in MIC2 secretion is not due to a defect in protein synthesis. As observed by IFA, a reduced level of constitutive GRA1 secretion was also

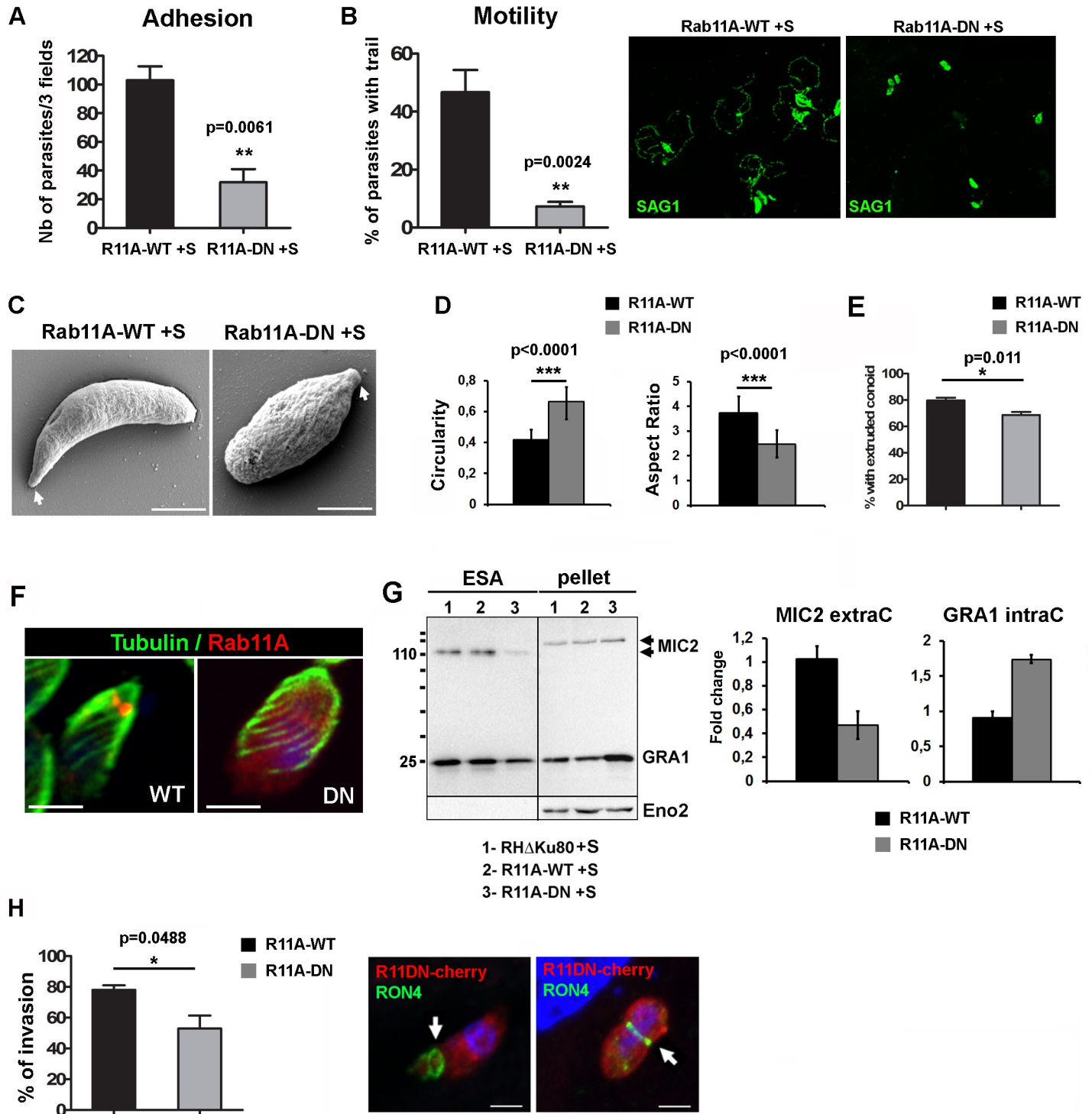


Fig 5. A- Quantification of Shield-1 induced extracellular Rab11A-WT and Rab11A-DN parasites adhering to host cells. Data indicate the number of parasites / 3 fields and show mean \pm SEM of three independent experiments (unpaired Student's *t*-test ** $p = 0.0061$). B- Quantification of the percentage of Shield-1 induced extracellular Rab11A-WT and Rab11A-DN parasites displaying a SAG1-positive trail deposit (green) as illustrated in the right images. Data show mean \pm SEM of three independent experiments (unpaired Student's *t*-test ** $p = 0.0024$). C- Scanning Electron Micrographs (SEM) of Shield-1 induced extracellular Rab11A-WT and Rab11A-DN parasites, which were allowed to move for 15 min on BSA-coated coverslips before fixation. Arrows indicate the apical pole of the parasite. Bars: 2 μ m. D- The histograms indicated the mean Circularity and Aspect Ratio (major axis / minor axis) of Shield-1 induced extracellular Rab11A-WT and Rab11A-DN parasites imaged by SEM ($n = 70$ parasites

for each condition; unpaired Student's *t*-test *** $p < 0.0001$). E- Histogram showing the percentage of Shield-1 induced Rab11A-WT and Rab11A-DN extracellular parasites displaying an extruded conoid (unpaired Student's *t*-test * $p = 0.011$). F- IFA showing the localization of the sub-pellicular microtubule network (green) in Shield-1 induced Rab11A-WT and Rab11A-DN (red) parasites. Bars: 2 μm . G- Western blot analysis of excreted-secreted antigen assays (ESA) performed with Shield-1 induced (+S) extracellular RHAKU80, Rab11A-WT and Rab11A-DN expressing parasites revealed a defect in MIC2 and GRA1 protein secretion. Eno2 was used as a loading control. Secreted MIC2 proteins (ESA fraction) and intracellular GRA1 proteins (pellet fraction) were quantified from 3 independent experiments and expressed as fold-change compared to induced RHAKU80 parasites. H- Quantification of the percentage of Shield-1 induced extracellular Rab11A-WT and Rab11A-DN expressing parasites, which have invaded host cells. Data show mean \pm SEM of three independent experiments (unpaired Student's *t*-test * $p = 0.0488$). Fluorescence images show Shield-1 induced mcherryRab11A-DN (red) invading host cells, as illustrated by the moving junction positive for RON4 (green). Bars: 1 μm .

<https://doi.org/10.1371/journal.ppat.1008106.g005>

detected by WB, which correlated with GRA1 accumulation in the parasite pellet fraction (Fig 5G). Together, these data suggest that the defect of extracellular Rab11A-DN parasites in host cell adhesion and motility may be due to impaired MIC2 delivery to the PM.

Lastly, Rab11A-DN parasites that successfully adhered to the surface of host cells, displayed only a mild defect in host cell invasion (Fig 5H). This was supported by the observation of a correctly formed RON4-positive junction by invading Rab11A-DN parasites (Fig 5H).

Collectively, these data demonstrate that Rab11A promotes parasite invasion by regulating parasite motility and adhesion to host cells, but not the formation of the moving junction.

Rab11A-positive vesicles accumulate at the apical pole during parasite motility and host cell invasion

The active role of Rab11A in parasite motility and adhesion led us to explore the localization of Rab11A in motile extracellular and invading parasites. Live imaging of mcherryRab11A-WT revealed an unexpected polarized accumulation of Rab11A-positive vesicles at two main foci localized at the apical tip of extracellular adhering and motile parasites (Fig 6A, S14 Movie). Apical accumulation of Rab11A appeared to be prolonged during host cell invasion (Fig 6B, S15 Movie). Apically polarized localization of Rab11A in invading parasites was further confirmed in fixed parasites after labeling of the moving junction with RON4 (Fig 6C).

Rab11A regulates polarized secretion of DG content during parasite motility and host cell invasion

Next, we assessed whether Rab11A regulates the transport of DGs, not only during parasite replication (Fig 3) but also during parasite motility and invasion. Similarly to the live imaging data (Fig 6), we found Rab11A at two foci localized at the apex of extracellular parasites that had been allowed to move on coverslips prior to fixation (Fig 7A). These Rab11A foci co-localized with the DG protein GRA1 suggesting that Rab11A may regulate apical transport and/or anchoring of DGs at the apical pole of motile extracellular parasites. A similar co-recruitment of Rab11A and DGs at two apical foci was observed during host cell invasion (Fig 7B, white arrows and S5A Fig). Most importantly, we observed a complete inhibition of this polarized DG apical localization in extracellular motile Rab11A-DN parasites (Fig 7A) and during host cell invasion (Fig 7B and S5A Fig). This demonstrates that Rab11A regulates the apical accumulation of DGs during the early steps of parasite motility and entry into host cells.

Discussion

In this study, we unraveled an essential role of Rab11A in the delivery of transmembrane proteins to the parasite PM and the release of DG proteins into the vacuolar space during intracellular replication.

In other eukaryotic systems, Rab11A localizes to the endocytic recycling compartment (ERC) and has been implicated in trafficking of internalized receptors from the ERC to the

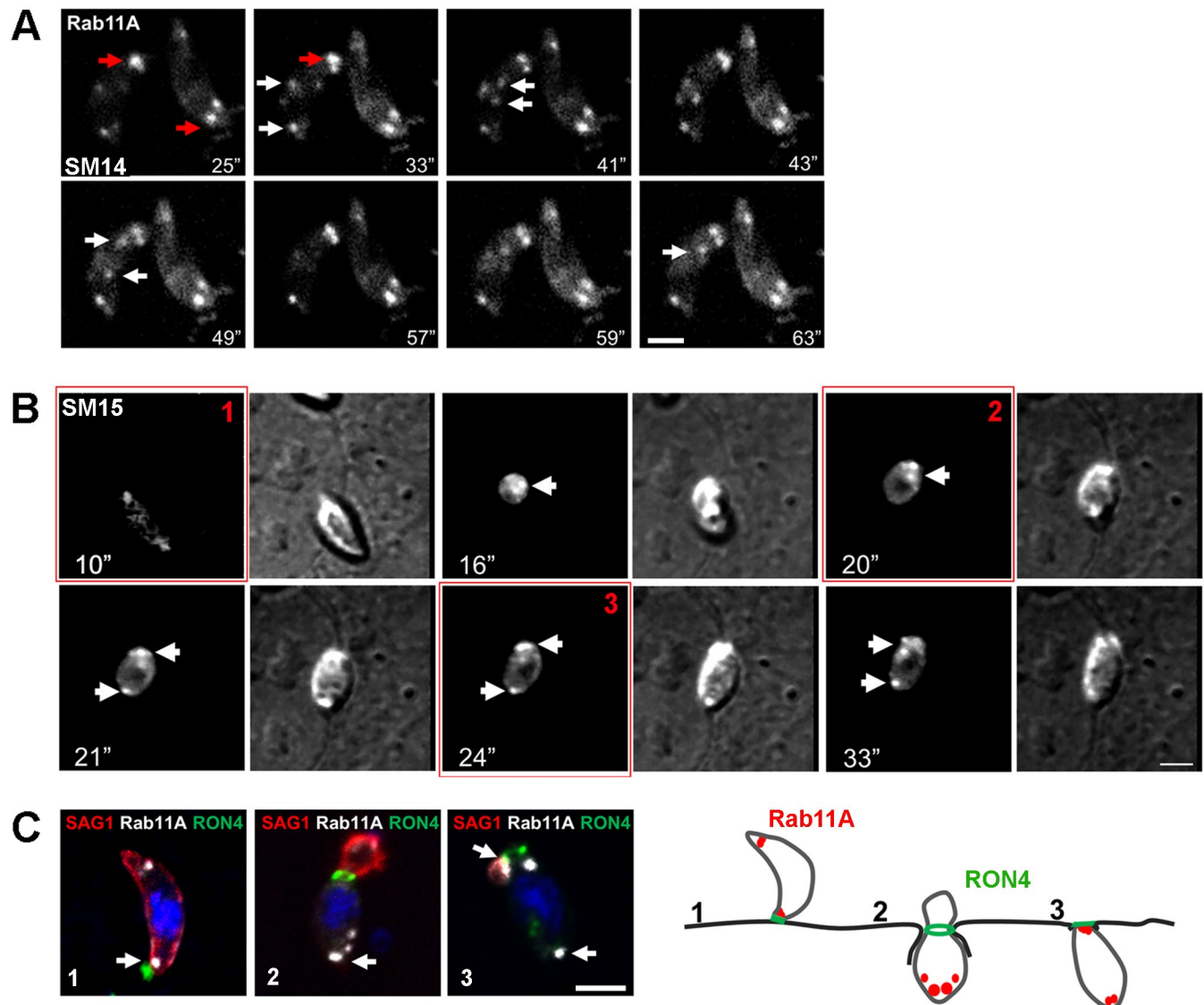


Fig 6. A- Sequences of images extracted from [S14 Movie](#) showing the polarized recruitment of mcherryRab11A-positive vesicles (white arrows) towards two main foci localized at the tip of adhering parasites (red arrows). Time is indicated in seconds. Bar: 2 μ m. B- Sequences of images extracted from [S15 Movie](#) showing a similar polarized localization of mcherryRab11A-positive vesicles (white arrows) during host cell invasion. At the end of parasite entry, Rab11A was also detected at the rear pole of the parasite. Time is indicated in seconds. Bar: 2 μ m. C-Fluorescence images of RH Δ KU80 parasites fixed at three different steps of the host cell invasion process, as indicated in the right scheme. The moving junction is labeled with RON4 (green) and the membrane protein SAG1 was used to label the extracellular portion of the invading parasite (red). Bar: 2 μ m.

<https://doi.org/10.1371/journal.ppat.1008106.g006>

PM [8]. Rab11A also localizes to the TGN compartment, where it regulates transport of material from this compartment to the ERC, or to the PM [17]. Similarly, during *T. gondii* cytokinesis, Rab11A mostly localizes at the Golgi of daughter cells, and at the tip of growing buds, suggesting a polarized transport of *de novo* synthesized material between these two locations during daughter cell emergence. Interestingly, a similar apically polarized localization of Rab11A was also evident during extracellular parasite motility. Thus, one may envision that components of the apical complex, a microtubule-rich structure from which emanates subpellicular microtubules [44], may control Rab11A-dependent recruitment of specific cargos at the apical pole of the parasite. In particular, RING2, a component of the apical polar ring, was

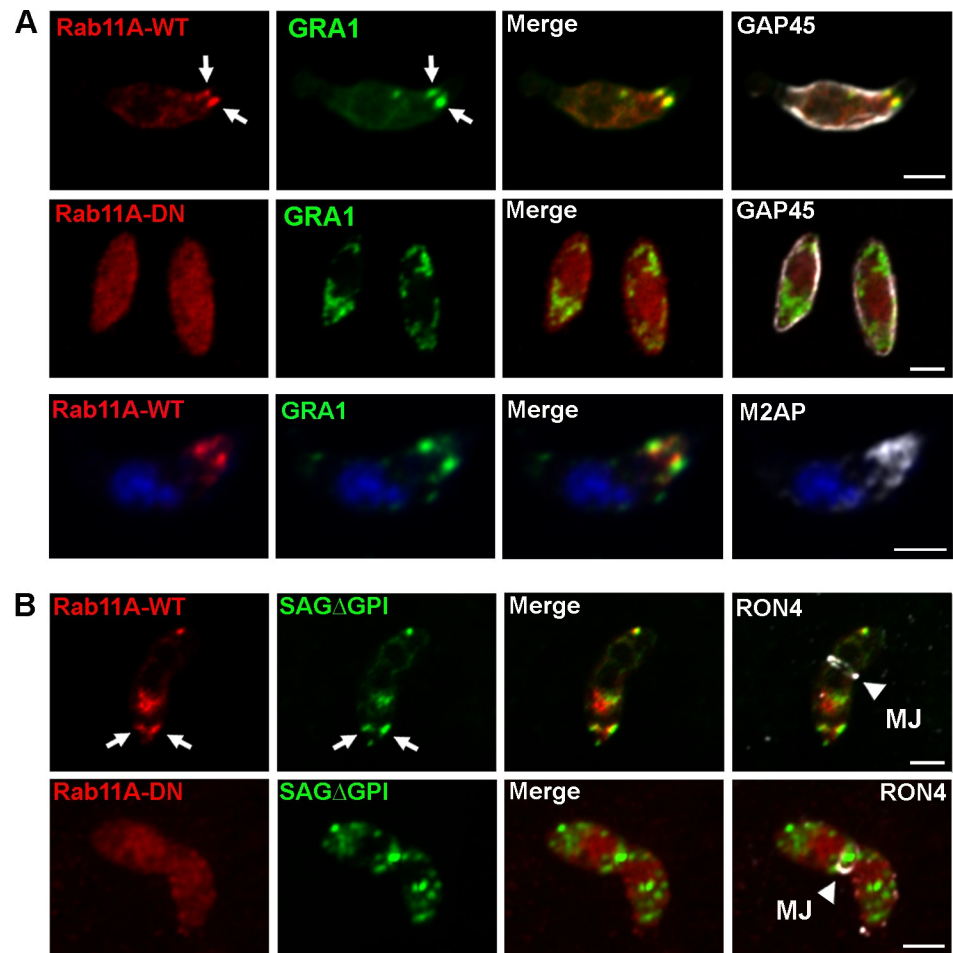


Fig 7. A- Immunofluorescence images showing the co-localization of mCherryRab11A (red) and GRA1-positive DGs (green) at two apical foci localized near the apical boundary of the Inner Membrane Complex (labeled with anti-GAP45 antibodies) in motile extracellular induced Rab11A-WT (upper row). This apically polarized accumulation is no longer detected in induced Rab11A-DN expressing parasites (middle row). The parasite apical pole is indicated by the presence of the microneme protein M2AP (lower row). Bars: 2 μ m. **B-** A similar apical and focalized co-localization between Rab11A and SAG Δ GPI-GFP-positive DGs (white arrows) is observed during host cell invasion confirmed by the detection of the RON4-positive moving junction. DG apical accumulation is no longer observed in invading Rab11A-DN. Bars: 2 μ m.

<https://doi.org/10.1371/journal.ppat.1008106.g007>

shown to function in constitutive and cGMP-stimulated secretion of microneme proteins [45]. Recently, two other components of the apical polar ring, APR1 and the Kinesin A, have also been reported to regulate MIC2 secretion [44]. Hence, it will be of interest to investigate whether Rab11A interacts with components of the apical polar ring to promote recruitment and/or exocytosis of micronemes and DG during extracellular motility and invasion.

Moreover, videomicroscopy recordings of mCherryRab11A-WT in intracellular parasites revealed highly dynamic Rab11A-positive vesicles displaying bidirectional trajectories between the apical and the basal poles, with an accumulation at the basal pole of replicating parasites. This suggests that Rab11A may contribute to the formation of the residual body, an organized structure that interconnects parasites during replication, or in the regulation of parasite exchanges, the two processes being likely tightly correlated. In this context, we observed Rab11A-positive vesicles and tubular-like structures in the region of the residual body. This region was recently reported to harbor a dense actin-myosin network that connects the

parasites within the PV ensuring synchronous divisions [6] [7]. Thus, Rab11A may also contribute to the regulation of this actin network function and dynamics. Indeed, in plants dysregulated Rab11A activity affects actin organization in the apical region of growing pollen tubes [46]. Supporting the hypothesis of a specific interaction between Rab11A and the actino-myosin cytoskeleton, depolymerizing actin filaments alters Rab11A-positive vesicle displacements. A role for the complex Myosin Vb-FIP2-Rab11A in promoting actin-mediated transport of vesicles has been previously observed in mammalian cells [47] [48] [49]. So far, no homologues of Rab11-family interacting proteins (FIPs) have been identified in *T. gondii* and *Plasmodium*. Nonetheless, *P. falciparum* Rab11A was reported to directly interact with the myosin light chain 1 (MLC1/MTIP), which therefore links Rab11A-mediated vesicular transport to unconventional myosins and the actin cytoskeleton [28]. As actin depolymerization resulted in the formation of both cytosolic and peripheral Rab11A-positive static clusters, it's possible that distinct myosins regulate different steps of Rab11A/DG transport e.g. MyoF in the cytosol and from the TGN [33], MyoA at the parasite cortex where the glideosome is located [28], and MyoJ in the cell-to-cell connecting network [6]. Further studies using parasite strains deleted for these molecular motors will address this question.

Co-distribution studies indicated that Rab11A-positive vesicles associate with dense granules in a dynamic manner. However, we did not observe Rab11A at the limiting membrane of DG. Rather, these two compartments appear to transiently dock one with each other enabling joint transient motions that were particularly evident at the cortex of the parasite. Indeed, tracking of the trajectories of both Rab11A-positive vesicles and DG revealed that Rab11A-positive vesicles promoted DG anchoring at the parasite cortex and their rapid “directed” transport. This mode of transport called “hitchhiking” has been recently described in different cell types and has emerged as a novel mechanism to control organelle movement [50]. During this process, the “hitchhiker” benefits from distinct molecular motors present at the surface of the “vehicle”. In addition, endosomes represent multifunctional platforms that receive specific signals and could drive transport of hitchhiker cargo to particular regions of the cell. Notably, co-movement of cargo may facilitate interactions at membrane contact sites important for organelle maturation, fusion and/or material exchange. Related to this last aspect, we found that over-expression of Rab11A-DN led to a complete block in DG secretion. We observed that restoration of Rab11A functions by washing out Shield-1 correlated with an accumulation of Rab11A-positive vesicles at the parasite plasma membrane suggesting a role for Rab11A in vesicle docking/tethering at the PM, which remains to be formally demonstrated. In other eukaryotic systems, Rab11A is known to promote vesicle docking and fusion at the PM via its interaction with the exocyst complex and SNARE proteins, respectively [15]. However, homologues of the different exocyst complex subunits could not be identified in *T. gondii* [51]. Thus, unexplored mechanisms of Rab11A-mediated vesicle docking at the PM may exist in *T. gondii* and Rab11A-interacting SNAREs remain to be identified. One may envision that Rab11A drives DGs to sites that favor exocytosis by promoting interactions with regulatory factors involved in vesicle fusion.

Benefiting from the fast and efficient induction of the Rab11A-DN protein expression in extracellular parasites, we confirmed the previously described defect in host cell invasion [30]. Of note, our numerous attempts to generate parasites expressing C-terminal tagged Rab11A failed, and notably, our attempts to apply the rapidly inducible AID knock-down system also failed [52]. This is likely due to the fact that the C-terminal domain of the Rabs contains one or two cysteines recognized by geranylgeranyl-transferases to induce their isoprenylation, a modification required for their association with membranes. The impaired cell invasion of Rab11A-DN expressing parasites results from a strong defect in parasite adhesion to host cells. Indeed, parasites that successfully adhered to host cells were only mildly perturbed in host cell

entry. Moreover, secretion of MIC2, an adhesin essential for parasite adhesion and motility was reduced upon dysregulation of Rab11A activity. Secretion of the GPI-anchored protein SAG1 is also altered in Rab11A-DN expressing parasites [28]. Thus, it's likely that the altered secretion of these two host cell adhesins contributes to the decrease in adhesion and motility of Rab11A-DN parasites. Consistent with a role of Rab11A in the regulation of surface protein trafficking, we also found a strong defect in the localization of the romboïd protease ROM4 and the glucose transporter GT1 at the PM, indicating a broader role of Rab11A in the regulation of surface protein trafficking. Presumably, distinct exocytic pathways exist in *T. gondii*, such as described in other organisms. In particular, whether a distinct endosome recycling compartment is present in *T. gondii* requires further exploration. Previous studies highlighted that *T. gondii* has functionally repurposed its endocytic system to serve as secretory pathway of this fast replicating intracellular parasite [51] [53]. In this context, the TGN appears to be a hybrid compartment to which the endosomal markers (Rab5 and Rab7) are tightly associated [31]. Therefore, one might envision that material internalized from the PM reaches this hybrid TGN/ELC compartment before being re-directed to other target membranes, such as the rhoptries, the PM, and the degradative vacuole (VAC). Such a recycling process has been recently observed during extracellular parasite motility [38]. Recycling of mother material during daughter cell emergence may also follow this indirect secretory pathway, while *de novo* synthesized proteins may traffic directly from the TGN to the PM.

Finally, during extracellular parasite motility and invasion, imaging of both live and fixed parasites revealed an unexpected polarized accumulation of Rab11A-positive vesicles towards two main foci located just beneath the conoid. In mammalian cells, Rab11A-dependent polarized secretion towards the leading edge of motile cells is essential to promote persistent migration [54]. This process not only provides additional membrane ensuring the extension of the leading edge, but also contributes to the translocation of regulatory factors involved in actin and microtubule cytoskeleton activity. In *T. gondii*, apical delivery of some effectors may regulate actin and microtubule cytoskeleton activity and thereby parasite motility. Such regulatory mechanisms have been demonstrated for the lysine methyltransferase, AKMT (Apical complex lysine (K) methyltransferase) localized at the conoid [55]. It has been also recently shown that the DG protein GRA8 contributes to parasite motility by regulating conoid extrusion and organization of the microtubule network [56]. Thus, future research will aim to identify the cargos that are apically delivered in a Rab11A-dependent manner and their putative role in regulating parasite motility. Interestingly, the apical accumulation of DGs that we observed in extracellular motile parasites has been previously described during parasite invasion [57]. Thus, an alternative explanation would be that the parasite “prepares its arrival” at the host cell, anticipating the burst of DG secretion that occurs during invasion by promoting their anchoring at the apical pole. In such a scenario, a second signal (vacuole closure?) would then trigger their fusion and content release into the vacuolar space.

Importantly, at present we cannot explain the defect in morphology we observed in extracellular motile Rab11A-DN parasites. This may be linked to a dysregulation of the actin cytoskeleton activity, or be related to a defect in the dynamics of an endo-exocytosis activity required for parasite forward movement, both potentially leading to shape deformation of the moving parasite. Along with the first hypothesis, actin staining (Cb-E transfected parasites) in extracellular parasites that were allowed to move on coated coverslips before fixation revealed a strong accumulation of actin at the basal pole of the parasite (S5B Fig), such as recently described in invading parasites [58].

Therefore, identifying Rab11A interactors will be an important future goal, as it will improve our understanding of the mechanisms regulating the distinct exocytic pathways in *T. gondii*. In particular, it will be important to characterize the molecular mechanisms involved

in anchoring Rab11A-positive vesicle to actin or microtubule molecular motors, and of a possible process of vesicle docking/tethering at the PM, both during parasite motility and intracellular replication. Finally, exploring a putative functional interaction between Rab11A and the apical complex may lead to the discovery of novel regulated secretory mechanisms essential to ensure parasite virulence.

Materials and methods

Parasite culture and transfection

Toxoplasma gondii Type I RH Δ KU80 Δ HXGPRT parasites were grown on confluent Human Foreskin Fibroblast (HFF) cells (CCD-112Sk (ATCC)) which were cultured in complete DMEM (gibcoLife Technologies) supplemented with 10% Fetal Bovine Serum (GibcoLife Technologies) and 1% Penicillin/Streptavidin (gibcoLife Technologies). To obtain the transgenic parasites, the RH Δ KU80 Δ HXGPRT parental strain was transfected by electroporation following standard procedures with 50 μ g of the plasmids listed in Table 1.

Following transfection, parasites were subjected to drug selection and verified for the transfection efficiency by immunofluorescence analysis. Subsequently the parasites were subjected to cloning by serial dilution.

Production of the anti-Rab11A antibodies

Recombinant purified GST-Rab11A protein was used to raise a TgRab11A specific mouse polyclonal antibody. The cleavage site present between the GST tag and Rab11A was digested with Precision protease (GE life science). GST-Rab11A bound to agarose beads was washed with 10 bed volumes of Cleavage buffer (50mM Tris HCl, pH7.0, 150mM NaCl, 1mM EDTA, 1mM DTT) at 4°C. Precision protease (40 units) was added to the cleavage buffer and incubated with the beads at 4°C overnight. The purified Rab11A was collected in the supernatant. 50 μ g of the purified recombinant protein suspended in Freund's Adjuvant were injected intraperitoneally into mice over a series of 4 boosts. Following the third boost, a sample of serum was collected and tested by western blot for antibody reactivity using a total protein extract of parasites. Once specific antibody activity was detected mice were sacrificed and serum collected and stored at -20°C.

Protein sample preparation and Western Blot

Parasites were lysed in a TritonX100 1%, NaCl 150mM, Hepes 10mM buffer and the lysate was loaded onto a 10% SDS polyacrylamide gel using. Proteins were blotted onto a nitrocellulose membrane and probed with the indicated primary antibodies followed by species-specific secondary antibodies conjugated with HRP. Antibodies were diluted in 5% milk dissolved in TNT buffer (0.1M Tris HCl pH7.6, 0.15M NaCl and 0.1% v/v Tween20). The probed nitrocellulose membranes were visualized using the ECL Western blotting substrate (Pierce).

Table 1. List of plasmids used for parasite transfection.

Plasmid	Selection	Laboratory
DD-cmycmcherry-Rab11A-WT	HXGPRT	Meissner M [26]
DD-cmycmcherry-Rab11A-DN	HXGPRT	Meissner M [26]
IMC3-YFP	DHFR	Gubbels MJ
SAG1 Δ GPI-GFP	CAT	Heaslip A [31]
pLic GRA16-HA	DHFR	MA Hakimi [33]

<https://doi.org/10.1371/journal.ppat.1008106.t001>

Immunofluorescence assay

Confluent HFF monolayers were grown on coverslips and infected with parasites prior to fixing with 4% PFA for 15 min. After quenching with 50mM NH₄Cl, the coverslips were permeabilized with 0.2% triton dissolved in 5% FBS-PBS for 30 min. Coverslips were incubated with primary antibodies in 0.1% triton dissolved in 2% FBS-PBS and then washed thrice with 1X PBS. Alternatively, the coverslips were incubated with primary antibodies in 0.01% Saponin diluted in 2%FBS-PBS for 1 h. Incubation with secondary antibodies was performed in 0.1% triton or 0.01% Saponin dissolved in 2%FBS-PBS for 30 min. To label invading parasites, freshly egressed extracellular parasites expressing Rab11A-WT and Rab11A-DN were induced with Shield-1 for 2 h and seeded onto HFF monolayers in a 24-well plate at a concentration of 2×10^6 parasites (Rab11A-WT) and 4×10^6 (Rab11A-DN) /500 μ l complete medium containing Shield-1 per coverslip. The plate was centrifuged for 2 min at 1000rpm at room temperature to trigger adhesion and synchronized invasion events. The plate was immediately shifted to a water bath at 37°C and the parasites were fixed with 4% PFA-sucrose at the following time points—0, 2 and 5 min. Coverslips were washed with PBS and adherent or invading parasites labeled without permeabilization with the anti-SAG1 antibody and a secondary anti-mouse AlexaFluor405 antibody. After washing with PBS, parasites were permeabilized with 0.05% saponin for 10 min, followed by a blocking step with 5% FBS-PBS for 30 min. Next, coverslips were incubated with rabbit anti-RON4 antibodies and secondary anti-rabbit AlexaFluor488 to label the moving junction. Depending on the experiment, additional primary antibodies were added to detect GRA1, GRA3 and Rab11A during parasite invasion. Images were acquired using a Zeiss LSM880 confocal microscope equipped with an airyscan module. The antibodies used in this study are listed in [Table 2](#).

Table 2. List of antibodies.

Antibody M: Mouse Rb: Rabbit	Dilution (IFA)	Origin
anti-Rab11A-M	1/250	our lab
anti-SAG1-M	1/200	our lab
anti-GRA1-M	1/500 and 1/1000 WB	Biotem
anti-GRA3-Rb	1/200	JF. Dubremetz
anti-HA-Rb	1/400	Cell Signaling Technology
anti-cMyc-rat	1/400	Abcam
anti-GAP45-Rb	1/5000	D. Soldati Favre
anti-MIC2-M	1/200 and 1/500 WB	V. Carruthers
anti-ROP2_3-M	1/500	JF. Dubremetz
anti-GRA2-M	1/500	Biotem
anti-GRA5-M	1/500	Biotem
anti-IMC3-Rb	1/300	MJ. Gubbels
anti-RON4-Rb	1/500	M. Lebrun
anti-Ty-M	1/20	D. Soldati Favre
anti-M2AP-Rb	1/300	V. Carruthers
anti-sortilin-rat	1/1000	our lab
anti-tubulin-M	1/300	Sigma Life Sciences
anti-Eno2-Rb	1/1000 WB	our lab

<https://doi.org/10.1371/journal.ppat.1008106.t002>

Invasion assay

Freshly egressed extracellular parasites expressing Rab11A-WT and Rab11A-DN were harvested and treated for 2 h with 1 μM of Shield-1. Induced parasites were counted and seeded onto HFF monolayers in a 24-well plate at a concentration of 2×10^6 parasites (Rab11A-WT) or 4×10^6 parasites (Rab11A-DN) / 500 μl complete medium containing Shield-1 / coverslip. The plate was centrifuged for 2 min at 1000rpm at RT to trigger immediate adhesion and synchronized invasion events. Parasites were then shifted to 37°C for 1 h. The coverslips were washed with PBS—three times prior to fixation. Cells were fixed in 4% PFA for 10 min and subjected to a red/green invasion assay. Briefly, adherent external parasites were labeled without permeabilization with mouse anti-TgSAG1 antibodies, followed by secondary anti-mouse antibodies coupled to Alexa488. After cell permeabilization with TritonX100 0.1%, invaded intracellular parasites were detected using rabbit anti-TgGAP45 antibodies followed with a secondary anti-rabbit antibodies coupled to Alexa594. All parasites labeled green-red were considered as extracellular, while parasites exclusively red (positive for GAP45) were considered intracellular. At least 300 parasites were counted for each condition performed in triplicate. Data represent mean values \pm SEM from three independent biological experiments.

Motility (Trail deposition) Assay

Glass slides were coated with 100 $\mu\text{g/ml}$ BSA-PBS and incubated at 37°C for 1 h. The slides were washed three times with PBS and allowed to dry. Freshly egressed extracellular Rab11A-WT and Rab11A-DN expressing parasites were harvested and treated for 2 h with 1 μM of Shield-1. Induced parasites were counted and suspended in HHE buffer (HBSS, 10mM HEPES, 1mM EGTA) containing 1 μM of Shield-1. 1×10^6 (Rab11A-WT) or 2×10^6 (Rab11A-DN) parasites were seeded per well and incubated for 15 min at 37°C. Parasites were then fixed with 4% PFA in PBS for 10 min at RT. A standard IFA protocol was followed wherein primary mouse anti-SAG1 antibodies were used followed by goat anti-mouse secondary antibodies conjugated to Alexa Fluor 488. 200 parasites per coverslip were counted for the presence or absence of a SAG1-positive trail. With internal triplicates, the experiment was performed 3-times. Mean values \pm SEM was calculated.

Adhesion assay

Freshly egressed extracellular Rab11A-WT and Rab11A-DN parasites were harvested and treated for 2 h with 1 μM of Shield-1. Parasites were then counted and resuspended in Endo buffer (44.7mM K_2SO_4 , 10mM Mg_2SO_4 , 100mM sucrose, 5mM glucose, 20mM Tris, 0.35% wt/vol BSA—pH 8.2) containing 1 μM cytochalasin D and 1 μM of Shield-1. 2×10^6 parasites were then seeded onto confluent HFF cells grown on glass coverslips, spun down for 2 min at 1000rpm and incubated for 15 min at 37°C in the presence of 1 μM cytochalasin D and Shield-1. The coverslips were washed with PBS before fixation with PFA 4% for 10 min. The Red/Green assay was performed (see “Invasion assay”). At least 200 parasites were counted for each condition performed in triplicate. Data represent mean values \pm SEM from three independent biological experiments.

Conoid extrusion assay

Freshly egressed extracellular Rab11A-WT and Rab11A-DN parasites were harvested and treated for 2h with 1 μM of Shield-1. Parasites were then counted and resuspended in HS buffer (20mM HEPES, 138mM NaCl, 2.7mM KCl, 10% FBS—pH7.2). Conoid extrusion was induced with 2% ethanol for 30s and parasites were seeded on poly-L-lysine coverslips prior fixation

with PFA 4% in PBS. At least 100 parasites were counted for each condition performed in triplicate. Data represent mean values \pm SEM.

Excreted secreted antigens assay

50×10^6 freshly egressed extracellular Rab11A-WT and Rab11A-DN parasites were harvested and treated for 2 h with $1 \mu\text{M}$ of Shield-1. Shield-1 treatment was maintained throughout the experiment in all media. Parasites were mixed with an equal volume of pre-warmed intracellular (IC) buffer (5 mM NaCl, 142 mM KCl, 1 mM MgCl₂, 2mM EGTA, 5.6 mM glucose and 25 mM HEPES, pH 7.2) and spun down at 1500rpm, RT for 10 min. The pellet was washed once in the IC buffer under similar conditions and then resuspended in Egress buffer (142 mM NaCl, 5mM KCl, 1 mM MgCl₂, 1mM CaCl₂, 5.6 mM glucose and 25 mM HEPES, pH 7.2) containing 2% ethanol and incubated for 30 min at 37°C. The samples were spun down at 14000 rpm for 15 min at 4°C and the supernatant containing ESA saved. Pellets were washed once in 1x PBS and saved. The ESA and pellet fractions were suspended in 4x Laemelli blue buffer and subjected to Western blot as described above. The blots were probed with mouse anti-MIC2, mouse anti-GRA1 and rabbit anti-eno2 antibodies. Quantification has been performed using the ImageJ software.

Transmission electron microscopy (TEM)

After infection of a confluent HFF monolayer, cells containing replicating shield-1 induced Rab11A-WT and Rab11A-DN expressing parasites were detached with a scraper, spun down and fixed with 1% glutaraldehyde in 0.1 M sodium cacodylate pH 6.8 overnight at 4°C. Cells were post-fixed with 1% osmium tetroxide and 1.5% potassium ferricyanide for 1 h, then with 1% uranyl acetate for 45 min, both in distilled water at RT in the dark. After washing, cells were dehydrated in graded ethanol solutions then finally infiltrated with epoxy resin and cured for 48 hs at 60°C. Sections of 70–80 nm thickness on formvar-coated grids were observed with a Hitachi H7500 TEM (Elexience, France), and images were acquired with a 1 Mpixel digital camera from AMT (Elexience, France).

Scanning Electron microscopy (SEM)

Parasites were seeded on BSA coated-glass coverslips for 15 min at 37°C before being fixed with 2.5% glutaraldehyde in 0.1 M sodium cacodylate for 30 min. After washing, cells were treated with 1% osmium tetroxide in water, in the dark for 1 hour. Cells were dehydrated with increasing ethanol concentration baths. After two pure ethanol baths, cells were air-dried with hexamethyldisilazan (HMDS). Finally, dry coverslips were mounted on stubs and coated with 5 nm platinum (Quorum Technologies Q150T, Milexia, France) and cells were imaged at 2 kV by a secondary electron detector with a Zeiss Merlin Compact VP SEM (Zeiss, France).

The circularity and aspect ratio (AR) parameters were calculated using the ImageJ software. First, each parasite contour was manually delineated on the SEM images and the pluggin “Analyze”> “Set measurements”> Shape descriptor” was applied for all defined ROI (individual parasites, n = 70) to extract the circularity and aspect ratio parameters. Circularity describes how close an object is to a true circle and is calculated using the formula: $\text{circularity} = 4D^*(\text{area}/\text{perimeter}^2)$. A circularity value of 1 indicates a perfect circle. As the value approaches 0, it indicates an increasingly elongated shape. The aspect ratio describes the proportional relationship of an object’s width to its height and is calculated using the formula: $\text{AR} = \text{major axis}/\text{minor axis}$.

Videomicroscopy

Time-lapse video microscopy was conducted in LabTek chambers installed on an Eclipse Ti inverted confocal microscope (Nikon France Instruments, Champigny sur Marne, France) with a temperature and CO₂-controlled stage and chamber (Okolab), equipped with two Prime 95B Scientific Cameras (Photometrics, UK) and a CSU W1 spinning disk (Yokogawa, Roper Scientific, France). The microscope was piloted using MetaMorph software (Universal Imaging Corporation, Roper Scientific, France). A live-SR module (Gatca Systems, France) was added to the system to improve the obtained resolutions. Exposure time of 500 ms was used for the simultaneous acquisition of the GFP and mCherry channels, in dual camera mode (with band pass filters 525/50 nm and 578/105 nm, dichroic mirror at 560 nm, and laser excitation at 488 nm and 561 nm). Videos were captured at 2 frame/second.

Automatic tracking and vesicle co-distribution using the Imaris software

Automatic tracking of vesicles using the Imaris software (Bitplane, Oxford Instruments) was applied on the recorded videos retrieved from the GFP and mcherry channels of SAGΔG-PI-GFP / mcherryRab11A-WT expressing parasites. We first used the tool “Spot detector” for selecting-filtering spot size and intensity values for each channel. Next, we manually removed detection of false GFP-positive spots (notably detected in the vacuolar space due to the secretion of the SAGΔGPI protein). The tool “Track Manager” was used to manually correct the obtained tracks when required and to extract the xy positions of a given spot over time enabling to calculate the Mean Square Displacement (MSD) using MATLAB (see below). The tool “spot co-localization” was used to calculate the percentage of co-distribution between DG and Rab11A-positive vesicles. A distance of 300 nm between the spots was selected corresponding to the average size of the vesicles. At a given time point and for the entire vacuole, the number of all detected green spots, as well as the number of green spots co-distributing with the red spots were extracted to calculate the co-distribution percentage. This was repeated over 5 consecutive time points every 2 s for the first 10 s of recording to avoid bleaching of the fluorescent signals. The mean co-distribution percentage over these 5 time points was calculated per vacuole. The mean +/- SD of 10 vacuoles was then calculated.

Manual tracking and mathematical modeling with MATLAB

When indicated, the manual tracking plugin from the ImageJ software (<https://imagej.nih.gov/ij/>) was applied on the images obtained with the MetaMorph software to extract in time the spatial xy positions of the fluorescent vesicles. In order to track and model the type of motion of the vesicle, images were processed in MATLAB (www.mathworks.com) by applying *fit* function (‘poly1’ or ‘poly2’ options).

MSD was calculated thanks to a MATLAB script according to the formula:

$$MSD(n\Delta t) = \frac{1}{N-n} \sum_{i=1}^{N-n} (d_{i+n} - d_i)^2$$

MSD curves were fitted according to the formula:

- $MSD = 4Dt + v^2t$ (with D the Diffusion Coefficient and v the velocity), for directed motion
- $MSD = 4Dt$ (with D the Diffusion Coefficient), for normal diffusion.

Statistics

Means and SEM / SD were calculated in GraphPad (Prism). *P*-values were calculated using the Student's *t*-test assuming equal variance, unpaired samples and using two-tailed distribution.

Supporting information

S1 Fig. IFA showing the localization of Rab11A (red), the TGN marker *TgSORTLR* and the ELC marker *TgRab5A* (green) in fixed RHΔKU80 parasites during the G1 phase of the cell cycle (A) and cytokinesis (B). Parasite contours or daughter cells buds are revealed after detection of the protein IMC3 (white). Zooms of the areas indicated by white frames (1, 2) and corresponding to the Golgi/ELC region of a given parasite are also shown. The image B^s originating from a separate vacuole illustrates the localization of Rab11A at the tip of the forming daughter cell buds. Bars: 2 μm.

(TIF)

S2 Fig. A-Immunofluorescence assay showing the dense granule proteins GRA2 and GRA5 (green) retained in intra-cytosolic vesicles in Shield-1-induced (+S) Rab11A-DN expressing parasites, while being efficiently released into the vacuolar space and at the vacuole membrane in induced Rab11A-WT expressing parasites. The parasite cortex is delineated by GAP45 (red). Bars: 2 μm. **B-** Fluorescence images showing the dense granule protein GRA16 (green) retained in intra-cytosolic vesicles in Shield-1-induced Rab11A-DN expressing parasites, while being secreted and translocated into the host cell nuclei (small arrows) in induced Rab11A-WT expressing parasites. Bars: 5 μm.

(TIF)

S3 Fig. A-Immunofluorescence assay showing the cortical localization of SAG1, GAP45 and MLC1 in Shield-1-induced extracellular adherent Rab11A-DN expressing parasites. Bars: 2 μm.

(TIF)

S4 Fig. Immunofluorescence images showing a similar localization of apical MIC2-positive micronemes (A) and of the plasma membrane protein ROM4 (B) in Shield-1 induced Rab11A-WT and Rab11A-DN parasites. Bars: 2 μm.

(TIF)

S5 Fig. A- Immunofluorescence images showing the co-localization of the mcherryRab11A-positive signal (red) and GRA1-positive DG (green) at two apical foci in invading Rab11A-WT parasites. **B-** Immunofluorescence images showing the apical localization of mcherryRab11A (red) and the enrichment of actin (Cb-E, green) at the posterior pole of motile extracellular Rab11A-WT parasites. Bars: 2 μm.

(TIF)

S1 Movie. mcherryRab11A-positive vesicle (red) dynamics (left panel) in intracellular *T. gondii* parasites expressing IMC3-YFP (green). Imaging speed: 2 fps.

(AVI)

S2 Movie. mcherryRab11A-positive vesicle (red) dynamics (left panel) in intracellular *T. gondii* parasites expressing IMC3-YFP (green). Imaging speed: 2 fps.

(AVI)

S3 Movie. Movie showing mcherryRab11A-positive vesicles (left panel, arrows) moving along the developing daughter buds labeled with IMC3-YFP (right panel) during the process of

cytokinesis. Imaging speed: 2 fps.
(AVI)

S4 Movie. mcherryRab11A-positive vesicle (red) dynamics (left panel) at the basal pole of intracellular replicating *T. gondii* parasites. Imaging speed: 2 fps.
(AVI)

S5 Movie. mcherryRab11A-positive vesicle (red) dynamics in intracellular *T. gondii* parasites expressing Cb-Emerald GFP (green) showing a mcherryRab11A-positive vesicles moving along cortical F-actin. Imaging speed: 2 fps.
(AVI)

S6 Movie. Rab11A-positive vesicles (red) in close contact with dynamic cytosolic actin filaments in intracellular *T. gondii* parasites expressing Cb-Emerald GFP (green). Imaging speed: 2 fps.
(AVI)

S7 Movie. mcherryRab11A-positive vesicle (red) dynamics in intracellular *T. gondii* parasites treated with cytochalasin D for 30 min before imaging. Imaging speed: 2 fps.
(AVI)

S8 Movie. Movie showing the joint transport of a DG (green) docked on a Rab11A-positive vesicle (red) along the cortex of a SAG1ΔGPI-GFP and mcherryRab11A-WT expressing parasite followed by their automatic tracking.
(AVI)

S9 Movie. Automatic tracking of DG motion in SAG1ΔGPI-GFP expressing parasites.
(AVI)

S10 Movie. Movie showing 3 DG tracks extracted from a region of interest of SM9 and analyzed for their mode of motion. Trajectory 2 (also shown in SM8) displays a directed motion, while trajectories 1 and 3 display confined motions.
(AVI)

S11 Movie. Dense granule (green) dynamics in intracellular *T. gondii* parasites expressing SAG1ΔGPI-GFP and mcherryRab11A-DN. The trajectories of 4 DG were tracked.
(AVI)

S12 Movie. Dense granule (green) dynamics in intracellular *T. gondii* parasites expressing SAG1ΔGPI-GFP and mcherryRab11A-DN 4h after Shield-1 removing in 0,5 μM pre-induced Rab11ADN parasites. Imaging speed: 4 fps.
(AVI)

S13 Movie. Dense granule (green) dynamics in intracellular *T. gondii* parasites expressing SAG1ΔGPI-GFP and mcherryRab11A-DN 4h after Shield-1 removing in 1 μM pre-induced Rab11ADN parasites. Imaging speed: 2 fps.
(AVI)

S14 Movie. mcherryRab11A-positive vesicle (red) dynamics in Shield-1 induced extracellular motile *T. gondii* parasite. Imaging speed: 2 fps.
(AVI)

S15 Movie. mcherryRab11A-positive vesicle (left panel) dynamics in Shield-1 induced extracellular *T. gondii* parasite invading a host cell (right panel). Imaging speed: 2 fps.
(AVI)

Acknowledgments

We thank Aoife Heaslip, Marc-Jan Gubbels, Dominique Soldati-Favre, Jean-François Dubremetz, Maryse Lebrun and Ali-Mohamed Hakimi for sharing of reagents.

Author Contributions

Conceptualization: Kannan Venugopal, Syla Chehade, Sabrina Marion.

Formal analysis: Kannan Venugopal, Syla Chehade, Elisabeth Werkmeister, Nicolas Barois, Sabrina Marion.

Funding acquisition: Frank Lafont, Jamal Khalife, Gordon Langsley, Sabrina Marion.

Investigation: Kannan Venugopal, Nicolas Barois, Jamal Khalife, Gordon Langsley, Markus Meissner, Sabrina Marion.

Methodology: Kannan Venugopal, Syla Chehade, Elisabeth Werkmeister, Nicolas Barois, Javier Periz, Isabelle Tardieux, Markus Meissner, Sabrina Marion.

Project administration: Frank Lafont, Sabrina Marion.

Resources: Sabrina Marion.

Software: Elisabeth Werkmeister.

Supervision: Sabrina Marion.

Validation: Syla Chehade, Sabrina Marion.

Visualization: Sabrina Marion.

Writing – original draft: Kannan Venugopal, Syla Chehade, Sabrina Marion.

Writing – review & editing: Frank Lafont, Isabelle Tardieux, Jamal Khalife, Gordon Langsley, Markus Meissner.

References

1. Besteiro S, Dubremetz JF and Lebrun M. The moving junction of apicomplexan parasites: a key structure for invasion. *Cell. Microbiol.* 2011; 13, 797–805. <https://doi.org/10.1111/j.1462-5822.2011.01597.x> PMID: 21535344
2. Dubois DJ, Soldati-Favre D. Biogenesis and secretion of micronemes in *Toxoplasma gondii*. *Cell Microbiol.* 2019; 21:e13018. <https://doi.org/10.1111/cmi.13018> PMID: 30791192
3. The triumvirate of signaling molecules controlling *Toxoplasma* microneme exocytosis: Cyclic GMP, calcium, and phosphatidic acid. *Bullen HE, Bisio H, Soldati-Favre D. PLoS Pathog.* 2019; 15:e1007670. <https://doi.org/10.1371/journal.ppat.1007670> PMID: 31121005
4. Hakimi MA, Olias P, Sibley LD. *Toxoplasma* Effectors Targeting Host Signaling and Transcription. *Clin Microbiol Rev.* 2017; 30:615–645. <https://doi.org/10.1128/CMR.00005-17> PMID: 28404792
5. Muñoz-Hernández S, Carmen MG, Mondragón M, Mercier C, Cesbron MF, Mondragón-González SL, González S, Mondragón R. Contribution of the residual body in the spatial organization of *Toxoplasma gondii* tachyzoites within the parasitophorous vacuole. *J Biomed Biotechnol.* 2011; 2011:473983. <https://doi.org/10.1155/2011/473983> PMID: 22190852
6. Frénal K, Jacot D, Hammoudi PM, Graindorge A, Maco B, Soldati-Favre D. Myosin-dependent cell-cell communication controls synchronicity of division in acute and chronic stages of *Toxoplasma gondii*. *Nat Commun.* 2017; 8:15710. <https://doi.org/10.1038/ncomms15710> PMID: 28593938
7. Periz J, Whitelaw J, Harding C, Gras S, Del Rosario Minina MI, Latorre-Barragan F et al. *Toxoplasma gondii* F-actin forms an extensive filamentous network required for material exchange and parasite maturation. *Elife.* 2017; 6 pii: e24119. <https://doi.org/10.7554/eLife.24119> PMID: 28322189
8. Mercier C, Cesbron-Delauw MF. *Toxoplasma* secretory granules: one population or more? *Trends Parasitol.* 2015; 31:604. <https://doi.org/10.1016/j.pt.2015.02.002> PMID: 29496113

9. Katris NJ, Ke H, McFadden GI, van Dooren GG, Waller RF. Calcium negatively regulates secretion from dense granules in *Toxoplasma gondii*. *Cell Microbiol.* 2019; 21:e13011. <https://doi.org/10.1111/cmi.13011> PMID: 30673152
10. Grant BD and Donaldson JG. Pathways and mechanisms of endocytic recycling. *Nat Rev Mol Cell Biol.* 2009; 10: 597–608. <https://doi.org/10.1038/nrm2755> PMID: 19696797
11. Striepen B, He CY, Matrajt M, Soldati D, Roos DS. Expression, selection, and organellar targeting of the green fluorescent protein in *Toxoplasma gondii*. *Mol Biochem Parasitol.* 1998; 92:325–38. [https://doi.org/10.1016/s0166-6851\(98\)00011-5](https://doi.org/10.1016/s0166-6851(98)00011-5) PMID: 9657336
12. Striepen B, Soldati D, Garcia-Reguet N, Dubremetz JF and Roos DS. Targeting of soluble proteins to the rhoptries and micronemes in *Toxoplasma gondii*. *Mol Biochem Parasitol.* 2001; 92: 325–338.
13. Reiss M, Viebig N, Brecht S, Fourmaux MN, Soete M, Di Cristina M, et al. Identification and characterization of an escorter for two secretory adhesins in *Toxoplasma gondii*. *J Cell Biol.* 2001; 152:563–78. <https://doi.org/10.1083/jcb.152.3.563> PMID: 11157983
14. Stenmark H. Rab GTPases as coordinators of vesicle traffic. *Nat Rev Mol Cell Biol.* 2009; 10:513–25. <https://doi.org/10.1038/nrm2728> PMID: 19603039
15. Welz T, Wellbourne-Wood J, Kerkhoff E. Orchestration of cell surface proteins by Rab11. *Trends Cell Biol.* 2014; 24:407–15. <https://doi.org/10.1016/j.tcb.2014.02.004> PMID: 24675420
16. Campa CC and Hirsch E. Rab11 and phosphoinositides: A synergy of signal transducers in the control of vesicular trafficking. *Advances in Biological Regulation.* 2017; 63:132–139. <https://doi.org/10.1016/j.jbior.2016.09.002> PMID: 27658318
17. Chen W, Feng Y, Chen D, Wandinger-Ness A. Rab11 is required for trans-golgi network-to-plasma membrane transport and a preferential target for GDP dissociation inhibitor. *Mol. Biol. Cell.* 1998; 9:3241–3257. <https://doi.org/10.1091/mbc.9.11.3241> PMID: 9802909
18. Delevoye C, Miserey-Lenkei S, Montagnac G, Gilles-Marsens F, Paul-Gilloteaux P, Giordano F et al. Recycling endosome tubule morphogenesis from sorting endosomes requires the kinesin motor KIF13A. *Cell Rep.* 2014; 6:445–454. <https://doi.org/10.1016/j.celrep.2014.01.002> PMID: 24462287
19. Schuh M. An actin-dependent mechanism for long-range vesicle transport. *Nat Cell Biol.* 2011; 13:1431–6. <https://doi.org/10.1038/ncb2353> PMID: 21983562
20. Senye Takahashi S, Kubo K, Waguri S, Yabashi A, Shin HW, Katoh Y, Nakayama K. Rab11 regulates exocytosis of recycling vesicles at the plasma membrane. *Journal of Cell Science* 2012 125: 4049–4057. <https://doi.org/10.1242/jcs.102913> PMID: 22685325
21. Wu S, Mehta SQ, Pichaud F, Bellen HJ, Quirocho FA. Sec15 interacts with Rab11 via a novel domain and affects Rab11 localization in vivo. *Nat. Struct. Mol. Biol.* 2005; 12:879–85. <https://doi.org/10.1038/nsmb987> PMID: 16155582
22. Fielding AB, Schonteich E, Matheson J, Wilson G, Yu X, Hickson GR et al. Rab11-FIP3 and FIP4 interact with Arf6 and the exocyst to control membrane traffic in cytokinesis. *EMBO J.* 2005; 24:3389–99. <https://doi.org/10.1038/sj.emboj.7600803> PMID: 16148947
23. Westlake CJ, Baye LM, Nachury MV, Wright KJ, Ervin KE, Phu L. Primary cilia membrane assembly is initiated by Rab11 and transport protein particle II (TRAPP II) complex-dependent trafficking of Rabin8 to the centrosome. *Proc. Natl. Acad. Sci. U. S. A.* 2011; 108:2759–64. <https://doi.org/10.1073/pnas.1018823108> PMID: 21273506
24. Wilson GM, Fielding AB, Simon GC, Yu X, Andrews PD, Hames RS et al. The FIP3-Rab11 protein complex regulates recycling endosome targeting to the cleavage furrow during late cytokinesis. *Mol Biol Cell.* 2005; 16:849–860. <https://doi.org/10.1091/mbc.E04-10-0927> PMID: 15601896
25. Assaker G, Ramel D, Wculek SK, González-Gaitán M, Emery G. Spatial restriction of receptor tyrosine kinase activity through a polarized endocytic cycle controls border cell migration. *Proc. Natl. Acad. Sci. U. S. A.* 2010; 107:22558–63. <https://doi.org/10.1073/pnas.1010795108> PMID: 21149700
26. Kessler D, Gruen GC, Heider D, Morgner J, Reis H, Schmid KW et al. The action of small GTPases Rab11 and Rab25 in vesicle trafficking during cell migration. *Cell Physiol Biochem.* 2012; 29:647–56. <https://doi.org/10.1159/000295249> PMID: 22613965
27. Kremer K, Kamin D, Riittweger E, Wilkes J, Flammer H, Mahler S et al. An overexpression screen of *Toxoplasma gondii* Rab-GTPases reveals distinct transport routes to the micronemes. *PLoS Pathog.* 2013; 9:e1003213 <https://doi.org/10.1371/journal.ppat.1003213> PMID: 23505371
28. Agop-Nersesian C, Naissant B, Ben Rached F, Rauch M, Kretzschmar A, Thiberge S et al. Rab11A-controlled assembly of the inner membrane complex is required for completion of apicomplexan cytokinesis. *PLoS Pathog.* 2009; 5:e1000270. <https://doi.org/10.1371/journal.ppat.1000270> PMID: 19165333

29. Burke JE, Inglis AJ, Perisic O, Masson GR, McLaughlin SH, Rutaganira F et al. Structures of PI4KIII β complexes show simultaneous recruitment of Rab11 and its effectors. *Science*. 2014; 344:1035–8. <https://doi.org/10.1126/science.1253397> PMID: 24876499
30. McNamara CW, Lee MC, Lim CS, Lim SH, Roland J, Simon O et al. Targeting Plasmodium PI(4)K to eliminate malaria. *Nature*. 2013; 504:248–253. <https://doi.org/10.1038/nature12782> PMID: 24284631
31. Venugopal K, Werkmeister E, Barois N, Saliou JM, Poncet A, Huot L, Sindikubwabo F, Hakimi MA, Langsley G, Lafont F, Marion S. Dual role of the *Toxoplasma gondii* clathrin adaptor AP1 in the sorting of rhoptry and microneme proteins and in parasite division. *PLoS Pathog*. 2017; 13:e1006331. <https://doi.org/10.1371/journal.ppat.1006331> PMID: 28430827
32. Andenmatten N, Egarter S, Jackson AJ, Jullien N, Herman JP, Meissner M. Conditional genome engineering in *Toxoplasma gondii* uncovers alternative invasion mechanisms. *Nat Methods*. 2013; 10:125–7 <https://doi.org/10.1038/nmeth.2301> PMID: 23263690
33. Heaslip AT, Nelson SR, Warshaw DM. Dense granule trafficking in *Toxoplasma gondii* requires a unique class 27 myosin and actin filaments. *Mol Biol Cell*. 2016; 27:2080–9. <https://doi.org/10.1091/mbc.E15-12-0824> PMID: 27146112
34. Wang Y, Jeong Y, Jhiang SM, Yu L, Menq CH. Quantitative characterization of cell behaviors through cell cycle progression via automated cell tracking. *PLoS One*. 2014; 9:e98762 <https://doi.org/10.1371/journal.pone.0098762> PMID: 24911281
35. Bougdour A, Durandau E, Brenier-Pinchart MP, Ortet P, Barakat M, Kieffer S, Curt-Varesano A, Curt-Bertini RL, Bastien O, Coute Y, Pelloux H, Hakimi MA Host cell subversion by *Toxoplasma* GRA16, an exported dense granule protein that targets the host cell nucleus and alters gene expression. *Cell Host Microbe*. 2013; 13:489–500. <https://doi.org/10.1016/j.chom.2013.03.002> PMID: 23601110
36. Pomel S, Luk FC, Beckers CJM. Host cell egress and invasion induce marked relocations of glycolytic enzymes in *Toxoplasma gondii* tachyzoites. *PLoS Pathog*. 2008; 4:e1000188 <https://doi.org/10.1371/journal.ppat.1000188> PMID: 18949028
37. Jeffrey S, Buguliskis, Fabien Brossier, Joel Shuman, Sibley L. David. Rhomboid 4 (ROM4) Affects the Processing of Surface Adhesins and Facilitates Host Cell Invasion by *Toxoplasma gondii*. *PLoS Pathog*. 2010; 6: e1000858. <https://doi.org/10.1371/journal.ppat.1000858> PMID: 20421941
38. Brossier F, Jewett TJ, Sibley LD, Urban S. A spatially localized rhomboid protease cleaves cell surface adhesins essential for invasion by *Toxoplasma*. *Proc Natl Acad Sci U S A*. 2005; 102:4146–51. <https://doi.org/10.1073/pnas.0407918102> PMID: 15753289
39. Sangaré LO, Alayi TD, Westermann B, Hovasse A, Sindikubwabo F, Callebaut I, Werkmeister E, Lafont F, Slomianny C, Hakimi MA, Van Dorsselaer A, Schaeffer-Reiss C, Tomavo S. Unconventional endosome-like compartment and retromer complex in *Toxoplasma gondii* govern parasite integrity and host infection. *Nat Commun*. 2016; 7:11191. <https://doi.org/10.1038/ncomms11191> PMID: 27064065
40. Gras S, Jimenez-Ruiz E, Klinger CM, Schneider K, Klingl A, Lemgruber L, Meissner M. An endocytic-secretory cycle participates in *Toxoplasma gondii* in motility. *PLoS Biol*. 2019; 17:e3000060. <https://doi.org/10.1371/journal.pbio.3000060> PMID: 31233488
41. Amiar S, Katris N J., Berry L., Dass S., Shears M. J., Brunet C. et al. Division and adaptation to host nutritional environment of apicomplexan parasites depend on apicoplast lipid metabolic plasticity and host organelle remodeling. *bioRxiv*. <https://doi.org/10.1101/585737>
42. Gras S, Jackson A, Woods S, Pall G, Whitelaw J, Leung JM, Ward GE et al. Parasites lacking the micronemal protein MIC2 are deficient in surface attachment and host cell egress, but remain virulent in vivo. *Wellcome Open Res*. 2017; 2:32. <https://doi.org/10.12688/wellcomeopenres.11594.2> PMID: 28630943
43. Whitelaw JA, Latorre-Barragan F, Gras S, Pall GS, Leung JM, Heaslip A et al. Surface attachment, promoted by the actomyosin system of *Toxoplasma gondii* is important for efficient gliding motility and invasion. *BMC Biol*. 2017; 15:1. <https://doi.org/10.1186/s12915-016-0343-5> PMID: 28100223
44. Leung JM, He Y, Zhang F, Hwang YC, Nagayasu E, Liu J et al. Stability and function of a putative microtubule-organizing center in the human parasite *Toxoplasma gondii*. *Mol Biol Cell*. 2017; 28: 1361–1378 <https://doi.org/10.1091/mbc.E17-01-0045> PMID: 28331073
45. Katris NJ, van Dooren GG, McMillan PJ, Hanssen E, Tilley L, Waller RF. The apical complex provides a regulated gateway for secretion of invasion factors in *Toxoplasma*. *PLoS Pathog*. 2014; 10:e1004074. <https://doi.org/10.1371/journal.ppat.1004074> PMID: 24743791
46. de Graaf BH, Cheung AY, Andreyeva T, Lévassieur K, Kieliszewski M, Wu HM. Rab11 GTPase-Regulated Membrane Trafficking Is Crucial for Tip-Focused Pollen Tube Growth in Tobacco. *Plant Cell*. 2005; 17:2564–2579. <https://doi.org/10.1105/tpc.105.033183> PMID: 16100336
47. Horgan CP, McCaffrey MW. The dynamic Rab11-FIPs. *Biochem Soc Trans*. 2009; 37:1032–6. <https://doi.org/10.1042/BST0371032> PMID: 19754446

48. Chu BB, Ge L, Xie C, Zhao Y, Miao HH, Wang J et al. Requirement of Myosin Vb-Rab11a-Rab11-FIP2 Complex in Cholesterol-regulated Translocation of NPC1L1 to the Cell Surface *J Biol Chem*. 2009; 284: 22481–22490 <https://doi.org/10.1074/jbc.M109.034355> PMID: 19542231
49. Schafer JC, Baetz NW, Lapierre LA, McRae RE, Roland JT, Goldenring JR. Rab11-FIP2 Interaction with MYO5B Regulates Movement of Rab11a-Containing Recycling Vesicles. *Traffic*. 2014; 15: 292–308 <https://doi.org/10.1111/tra.12146> PMID: 24372966
50. Salogiannis J, Reck-Peterson SM. Hitchhiking: A Non-Canonical Mode of Microtubule-Based Transport. *Trends Cell Biol*. 2017; 27: 141–150. <https://doi.org/10.1016/j.tcb.2016.09.005> PMID: 27665063
51. Tomavo S, Slomianny C, Meissner M, Carruthers VB. Protein trafficking through the endosomal system prepares intracellular parasites for a home invasion. *PLoS Pathog*. 2013; 9:e1003629. <https://doi.org/10.1371/journal.ppat.1003629> PMID: 24204248
52. Brown KM, Long S, Sibley LD. Conditional Knockdown of Proteins Using Auxin-inducible Degron (AID) Fusions in *Toxoplasma gondii*. *Bio Protoc*. 2018; 8.pii: e2728 <https://doi.org/10.21769/BioProtoc.2728> PMID: 29644255
53. Venugopal K, Marion S. Secretory organelle trafficking in *Toxoplasma gondii*: A long story for a short travel. *Int J Med Microbiol*. 2018; 308:751–760. <https://doi.org/10.1016/j.ijmm.2018.07.007> PMID: 30055977
54. Fletcher SJ, Rappoport JZ. Moving forward: polarised trafficking in cell migration. *Trends Cell Biol*. 2010; 20:71–78. <https://doi.org/10.1016/j.tcb.2009.11.006> PMID: 20061150
55. Heaslip AT, Nishi M, Stein B, Hu K. The motility of a human parasite, *Toxoplasma gondii*, is regulated by a novel lysine methyltransferase. *PLoS Pathog*. 2011; 7:e1002201 <https://doi.org/10.1371/journal.ppat.1002201> PMID: 21909263
56. Díaz-Martín RD, Mercier C, Gómez de León CT, González RM, Pozos SG, Ríos-Castro E et al. The dense granule protein 8 (GRA8) is a component of the sub-pellicular cytoskeleton in *Toxoplasma gondii*. *Parasitol Res*. 2019; 118:1899–1918. <https://doi.org/10.1007/s00436-019-06298-7> PMID: 30949853
57. Labruyère E, Lingnau M, Mercier C, Sibley LD. Differential membrane targeting of the secretory proteins GRA4 and GRA6 within the parasitophorous vacuole formed by *Toxoplasma gondii*. *Molecular and Biochemical Parasitology*. 1999; 102:311–324. [https://doi.org/10.1016/s0166-6851\(99\)00092-4](https://doi.org/10.1016/s0166-6851(99)00092-4) PMID: 10498186
58. Del Rosario M, Periz J, Pavlou G, Lyth O, Latorre-Barragan F, Das S, Pall GS, Stortz JF, Lemgruber L, Whitelaw JA, Baum J, Tardieux I, Meissner M. Apicomplexan F-actin is required for efficient nuclear entry during host cell invasion. *EMBO Rep*. 2019; 20:e48896. <https://doi.org/10.15252/embr.201948896> PMID: 31584242